AIMS Mathematics, 10(12): 29189–29235.
DOI: 10.3934/math.20251284
Received: 28 October 2025
Revised: 19 November 2025
Accepted: 02 December 2025
Published: 11 December 2025

https://www.aimspress.com/journal/Math

Research article

Ion–acoustic waves in a conformable fractional mKdV framework: Solitons, periodic solutions, and Hirota bilinear construction

Khalid A. Alsatami*

Department of Mathematics, College of Science, Qassim University, Buraydah, Saudi Arabia

* **Correspondence:** Email: satamy@qu.edu.sa.

Abstract: The main aim of this study is to formulate a space–time fractional modified Korteweg–de Vries (mKdV) model for describing ion-acoustic wave propagation in magnetized, multi-component plasmas. By employing the conformable fractional derivative, we derive a reduced evolution equation and obtain exact traveling wave solutions through three complementary approaches: Integration, Jacobi elliptic constructions, and a Hirota bilinear formulation. These methods yield soliton, kink, and periodic wave families, while the associated phase portraits characterize the corresponding dynamic regimes. The fractional order α systematically modulates the amplitude and width of the solutions, with the classical mKdV limit recovered smoothly as $\alpha=1$. The findings provide a physically transparent fractional framework together with analytical benchmark solutions that will be useful for validating numerical solvers and interpreting nonlinear structures in laboratory and space plasmas.

Keywords: partial differential equations; space–time fractional mKdV; ion-acoustic waves; magnetized multi-component plasma; traveling waves; Hirota bilinear method; phase portrait and bifurcation analysis
Mathematics Subject Classification: 34A34, 34C15, 34C25, 35L65, 37N30

Table 1 summarizes all abbreviations and symbols used throughout the manuscript.

Table 1. List of abbreviations and symbols.

Abbreviation	Meaning	Abbreviation	Meaning
KdV	Korteweg–de Vries	**mKP**	Modified Kadomtsev–Petviashvili
mKdV	modified Korteweg–de Vries	**ZK**	Zakharov–Kuznetsov
CFD	Conformable fractional derivative	**stf**	Space–time fractional
RPM	Reductive perturbation method	n_c, n_e	Number density of cool electrons and hot electrons
IASWs	Ion acoustic solitary waves	u	Ion flow velocity
ODE	Ordinary differential equation	φ	Ion pressure, electrostatic potential
PDE	Partial differential equation	$q=n_{c0}/n_{i0}$	Ratio of the equilibrium of cool electron density to ion density
KP	Kadomtsev–Petviashvili	n_0	The equilibrium electron density
α	Fractional order	V_0, k, ω	Phase velocity, wave number, and wave frequency
A, B	Nonlinear dispersive coefficients	B_0	The external magnetic field
MEW	Modified equal width		
AKNS	Ablowitz-Kaup-Newell-Segur	***NLS***	Nonlinear Schrodinger
FDE	Fractional differential equation	***sn, cn, dn***	Elliptic sine, elliptic cosine, delta amplitude functions

1. Introduction

The study of ion acoustic solitary structures has occupied a central position in plasma physics since the seminal work of Washimi and Taniuti, who first demonstrated that weakly nonlinear ion acoustic disturbances evolve according to the KdV framework and support stable solitary waves [1]. Subsequent developments have extended this foundational theory to a broad variety of plasma environments (including relativistic, magnetized, multi-component, and nonthermal systems) revealing that the morphology, polarity, and stability of solitary waves are highly sensitive to the ambient plasma's composition and equilibrium parameters. For example, ion acoustic propagation in relativistic or electron–positron–ion media undergoes substantial alterations due to charge symmetry, relativistic inertia, and the magnetic field's orientation [2–4]. Additionally, the incorporation of nonthermal electrons and positrons results in enhanced soliton families and dressed structures that are absent in Maxwellian plasmas [5–7]. Further improvements have considered degeneracy effects [8], curved geometries and shock-type behavior [9], and the way magnetized electron–positron–ion combinations move in an oblique direction [10]. These models are not only of theoretical interest but are also central to understanding astrophysical and space plasma processes, including magnetic field generation and nonlinear energy transport in strongly magnetized cosmic environments [11].

Recent studies have expanded the focus to multi-component environments characterized by positron-acoustic or dust-acoustic modes [12], resulting in shock structures [13], rogue waves, and multi-soliton interactions in plasmas with nonthermal or electron-depleted populations [14–16]. Concurrent investigations have examined nonlinear wave modulation inside generalized statistics or nonextensive electron distributions [17], revealing the formation of double layers, amplitude modulation, and intricate envelope dynamics in non-Maxwellian systems [18–20]. Ion acoustic wave propagation in electron–positron–ion setups has similarly unveiled several nonlinear characteristics, including intensified solitary pulses and complex phase-shift dynamics during solitons' interactions [21,22]. Contemporary

research has used sophisticated analytical methods, including the Hirota bilinear methodology, to elucidate multi-soliton generation and interaction in magnetized plasmas characterized by nonextensive electron populations [23]. This collection of literature emphasizes the universality and extensive variety of nonlinear wave events in plasma systems, while also stressing the persistent need for generalized models that can include nonlocality, anomalous transport, and fractional-order effects.

A broad spectrum of recent research across applied mathematics, nonlinear optics, biological transport, and stochastic modeling has demonstrated that the KdV-, mKdV-, and KP-type equations remain the fundamental descriptors of coherent structures in complex media. Studies on generalized KP–MEW systems using bifurcation and dynamic systems analysis have clarified solitary and periodic wave branches [24], while fractional extensions have captured memory effects and anomalous diffusion in biological and ecological transport models with strong analytical–numerical agreement [25]. As water-wave and multi-dimensional dispersive systems have gotten better at the same time, single waves, lump structures, and complex interaction dynamics [26–28] have been created. The Hirota bilinear scheme for making multi-soliton and resonance solutions [29–31]vis an example of how success in symbolic methods has made these changes even better. New developments in nonlinear optics and higher-order NLS models show that the processes of making solitons and interacting with them are the same in a lot of different physical settings [32–34].

New study is focusing on random effects, which change the solitons' amplitude, coherence, and stability in systems that are spread out and subject to changes in their surroundings [31–33]. The results of deterministic, fractional, and stochastic studies [34–36] show that we still need three things: (i) Generalized models that can show nonlocality and strange dispersion; (ii) exact analytical solutions that can be used to compare simulations and experiments; and (iii) frameworks that connect mathematical wave structures to physical signatures that can be seen. This study adds to the larger picture by creating a conformable fractional mKdV model that is consistent with dispersion and thus finding exact analytical traveling wave solutions that connect nonlinear theory with the conditions that are important to experiments in both the laboratory and space plasmas.

Recent advances in fractional calculus and nonlinear wave modeling further underscore the relevance of generalized evolution equations across physics, engineering, and applied mathematics. High-order numerical schemes (such as the local discontinuous Galerkin framework) have enabled accurate simulation of distributed-order and space–time fractional convection–diffusion [37,38] and Schrödinger-type systems [39,40], while local and fractal fractional derivatives have generated new exact wave structures in Vakhnenko–Parkes [41,42], Schrödinger, and related nonlinear equations [43,44]. Analytical methodologies including the first-integral, functional variable, Elzaki transform, and quasi-AKNS techniques have produced rich classes of solitary, periodic, and lump solutions for fractional NLS, KdV-type, and Burgers-like models [45–47], thereby extending the toolkit for handling nonlocality and anomalous dispersion. In astrophysics and fluids, fractional modeling has also been useful. It accurately describes polytropic gas spheres [48], Lane–Emden systems [49], and extended KdV equations where memory effects and scale-dependent transport are very important [50,51]. These studies show that fractional operators can be used to model nonlocal transport, strange diffusion, and complicated dispersive dynamics in a way that makes sense from a physical point of view. Exact analytical solutions are still needed for checking the numbers and figuring out what they mean physically.

This study adds to the body of research by creating a conformable fractional mKdV model for ion-acoustic waves that is consistent with dispersion. This model aligns analytical solvability with the physical modeling accuracy that is stressed in the fractional literature. Particularly influential for

applications is the conformable fractional derivative (CFD) introduced by Khalil et al. [50], which is defined through a limit-based extension

$$D^{\beta}\psi(x)=\lim_{\varepsilon\to 0}\frac{\psi(\mathrm{x}+\varepsilon x^{1-\beta})-\psi(\mathrm{x})}{\varepsilon}\quad \forall x>0,\ \beta\in(0,1],$$

$$\psi^{(\beta)}(0)=\lim_{x\to 0^{+}}\psi^{(\beta)}(x).$$

This preserves the core rules of standard calculus (linearity, product and chain rules, and a transparent reduction to the classical derivative as the order tends to one), and the CFD often enables direct transposition of integer-order analytical methods (exact solution techniques, symmetry reductions, and stability analyses) to fractional settings with minimal overhead.

$$D^{\beta}x^{n}=n\,x^{n-\beta},\ \ n\in\mathbb{R},\quad D^{\beta}a=0,\qquad \forall\psi(\mathrm{x})=a,$$

$$D^{\beta}(a\varphi+b\psi)=a\,D^{\beta}\varphi+b\,D^{\beta}\psi,\ \ \forall\ a,b\in\mathbb{R},$$

$$D^{\beta}(\varphi\psi)=\varphi D^{\beta}\psi+\psi D^{\beta}\varphi,$$

$$D^{\beta}\psi(\varphi)=\frac{d\psi}{d\varphi}D^{\beta}\varphi,\qquad D^{\beta}\varphi(x)=x^{1-\beta}\frac{d\varphi}{dx},$$

given that φ and ψ are two functions, while *a* and *b* are constants. This pragmatic balance between mathematical structure and computational tractability has facilitated a growing list of CFD-based applications, from wave and soliton dynamics in fractional NLS-type models [46,47] to astrophysical Lane–Emden-type equations and fractional polytropes [48], and to Burgers-like systems with fractional space–time geometry [49–51]. In what follows, we build on these developments to formulate, analyze, and solve fractional models of interest, while emphasizing regimes where conformable operators provide both theoretical clarity and efficient computation.

1.1. Problem statement and relevance

Ion-acoustic waves (IAWs) in magnetized, multi-component plasmas frequently display fractional order effects, anomalous transport, and superthermal particle populations that lie beyond the scope of classical integer-order models. Building on these observations, the attached work formulates and analyzes a space–time fractional mKdV model for a collisionless plasma composed of inertial ions and two nonextensive (cool/hot) electron populations in an external magnetic field. The central problem is to (i) derive a reduced fractional mKdV-type evolution equation that consistently incorporates locality and fractional order via conformable derivatives, (ii) characterize traveling waves (bright solitons, kink/antikink fronts, and periodic (Jacobi elliptic) wavetrains) together with their dependence on the fractional order α and physical coefficients, and (iii) establish the existence and phase-plane structure (homoclinic/heteroclinic/periodic orbits), including bifurcation scenarios and the effect of

weak time-periodic perturbations on dynamic behavior. A further objective is to compare the fractional dynamics with the classical limit by verifying that the solutions reduce to standard mKdV waves as $\alpha \to 1$.

This study is relevant to space and laboratory plasmas where non-Maxwellian electron populations and magnetization strongly influence electrostatic structures and their stability. Methodologically, it (a) derives the space–time fractional mKdV via a reductive perturbation scaling method tailored to conformable operators; (b) obtains exact solutions using complementary techniques (direct integration, Jacobi elliptic functions, Hirota bilinear construction for multi-soliton solutions, and Kudryashov and F-expansion methods), thereby furnishing analytically tractable waveforms across regimes; (c) quantifies the role of the fractional order α in modulating amplitude, width, and front steepness—showing systematic amplitude attenuation and profile broadening as α decreases; (d) classifies traveling waves through a Hamiltonian/phase-portrait analysis that links parameter sets to homoclinic (solitary), heteroclinic (kink/antikink), and periodic branches; and (e) outlines how weak nonautonomous forcing can seed complex responses beyond the integrable, autonomous core. Collectively, these results provide a coherent fractional-calculus framework that bridges theoretical modeling and observed solitary structures in magnetized, nonextensive plasmas and offers benchmark solutions for verification of numerical schemes and for designing experiments targeting controllable nonlinear wave dynamics.

1.2. Research objectives

This manuscript pursues seven integrated objectives: (i) To derive a self-consistent space–time fractional mKdV model for a magnetized, multi-component plasma using conformable fractional operators and reductive perturbation scaling; (ii) to establish the linear dispersion relation and verify classical consistency by showing reduction to the integer-order mKdV in the limit $\alpha \to 1$; (iii) to construct exact traveling wave solutions across regimes (including bright solitons, kink/antikink fronts, and Jacobi elliptic periodic wavetrains) complemented by Hirota's bilinear formulation for one- and two-soliton interactions; (iv) to perform a phase-space and bifurcation analysis of the traveling wave ODE to classify homoclinic, heteroclinic, and periodic orbits and delineate their transition boundaries; (v) to quantify the impact of the fractional order α and plasma parameters on the amplitude, width, and front steepness, with a systematic comparison with the classical benchmark; (vi) to assess robustness under weak external or parametric perturbations and document routes to complex dynamics; and (vii) to relate the theoretical predictions to observed ion acoustic structures and provide benchmark solutions for validating numerical solvers and guiding laboratory or space plasma experiments.

1.3. Novelty and differentiation

This work advances the state of the art along six fronts. (i) Fractional modeling with physical transparency: We derive a space–time mKdV model directly from laboratory variables, preserving a dispersion-consistent phase θ and making the roles of A (nonlinearity) and B (dispersion) explicit in the amplitudes, widths, and speeds (rather than hiding them behind canonical rescalings). (ii) A unified exact-solution toolkit for the fractional setting: Beyond the standard bright/kink one-solitons, we provide a coherent suite (Hirota bilinear (1- and 2-soliton in $(x,t;A,B)$), direct tanh/kink integration, and Jacobi elliptic (sn/cn/dn) wavetrains) with clear parameter maps and limiting connections (elliptic→

sech/tanh). (iii) Phase-space and bifurcation theory for fractional traveling waves: We carry out a Hamiltonian-style portrait and bifurcation classification (homoclinic, heteroclinic, periodic) in the fractional regime, quantifying how the order α deforms invariant sets and separatrices, and proving the consistency as α→1. (iv) Quantified α-dependence with design rules: We extract closed-form amplitude–speed–width scalings and monotone trends with α, yielding practical "knobs" for tuning solitary interfaces in plasma-relevant parameter ranges. (v) Interaction physics in physical units: Elastic two-soliton collisions (phase shifts, trajectories) are derived and reported directly in the form (*A,B*), enabling immediate comparison with experiments and simulations without retranslation from normalized forms. (vi) Reproducibility and benchmarking: We supply compact, ready-to-run MATLAB formulations for phase portraits and Hirota reconstructions, intended as benchmarks for numerical solvers of fractional PDEs and as templates for experimental fitting. Collectively, these elements differentiate the paper by unifying exact analysis, fractional calculus, and physically interpretable parametrizations into a single, application-ready framework.

1.4. Research gap justification

Despite extensive studies on ion acoustic solitary structures via classical (integer-order) KdV/mKdV frameworks, three substantive gaps persist. First, most fractional formulations are posed in normalized, canonical variables, obscuring how the physical coefficients (nonlinearity (*A*) and dispersion (*B*)) and the fractional order α jointly control the amplitude, width, speed, and phase; explicit, laboratory-unit parametrizations and dispersion-consistent phases have rarely been presented. Second, the literature offers few unified exact treatments of fractional traveling waves that span bright solitons, kink/antikink fronts, and Jacobi elliptic wavetrains, and even fewer that include multi-soliton Hirota constructions directly in (*x,t;A,B*) form with closed-form phase shifts. Third, rigorous phase-space and bifurcation analyses of the fractional traveling wave ODE quantifying how α deforms the equilibria, separatrices (homoclinic/heteroclinic), and periodic orbits, and proving consistency as α→1 remain underdeveloped, limiting interpretability and design utility. These gaps hinder principled comparisons with experiments and simulations, impede sensitivity studies in physically relevant parameter regimes, and deprive the community of benchmarkable, reproducible solution sets. The present work addresses these deficiencies by (i) deriving a dispersion-consistent mKdV model in physical units with transparent *A,B,α* dependence, (ii) furnishing a coherent exact solution toolkit (Hirota, direct integration, elliptic reductions) that unifies solitary and periodic branches and their limits, and (iii) delivering a quantitative phase portrait/bifurcation framework that links the fractional order to the observable waveform morphology and interaction outcomes.

1.5. Limitations of the proposed method

While the present work develops a unified and physically transparent space–time fractional mKdV framework, several limitations must be acknowledged to guide appropriate interpretation and future extensions. First, the use of the CFD (chosen for its compatibility with reductive perturbation, product and chain rules, and Hirota bilinearization) implies that the model remains local and therefore does not capture the genuine long-memory effects that are characteristic of Caputo, Riemann–Liouville, or Atangana–Baleanu operators. As such, the formulation is not suitable for

plasmas where history-dependent transport, nonlocality, or anomalous diffusion dominate. Second, the analysis is restricted to one-dimensional, weakly nonlinear ion-acoustic dynamics with long-wavelength reductive scaling; multi-dimensional geometries, kinetic resonances, strong Landau damping, and finite Larmor radius corrections are omitted. Third, the fractional order α is treated phenomenologically rather than derived from kinetic or experimental constraints, so parameter identification must be performed externally for specific plasma environments. Fourth, although the exact soliton, kink, cnoidal, and Hirota multi-soliton solutions are obtained analytically, their nonlinear stability under perturbations, noise, or coupling to additional plasma modes has not been investigated. Finally, the chaotic responses discussed in the presence of periodic forcing serve primarily as qualitative demonstrations; a full characterization of nonlinear stability and chaos (Lyapunov exponents, parameter continuation, global bifurcations) lies beyond the scope of the present study. These problems make it clear what needs to be studied next, such as creating nonlocal fractional plasma models, getting α from kinetic theory, looking at the stability and modulation of fractional solitons, and making multi-dimensional or magnetized generalizations that are useful for both laboratory and space plasma observations.

1.6. Verification of analytical solutions

To establish the correctness, internal consistency, and physical reliability of the analytical solutions obtained in this study, a multi-tiered verification framework is employed. First, each closed-form solution (solitary wave, kink/antikink structure, and Jacobi elliptic periodic waveforms) is substituted explicitly into both the reduced traveling wave ODE and the original space–time fractional mKdV equation. This direct substitution test confirms that all expressions satisfy the governing equations identically, thereby providing the strongest form of algebraic validation. Second, the fractional solutions are examined in the classical limit α=1, where the conformable fractional model must reduce smoothly to the standard integer-order mKdV equation. In this limit, the derived solutions recover the well-known sech-type solitons, tanh-type kinks, and Jacobi elliptic waveforms reported in the classical literature. This limiting case correspondence verifies that the fractional formulation is consistent with established nonlinear wave theory. Third, solutions generated through independent analytical approaches (including the Hirota bilinear method, direct quadrature, Kudryashov expansion, and reduction of the Jacobi elliptic function) are cross-compared. Under appropriate parameter identification, all techniques are shown to yield equivalent waveform structures, confirming methodological consistency across symbolic and nonsymbolic solution frameworks. Finally, for selected parameter regimes of physical relevance, the analytical solutions are benchmarked against numerical integrations of the fractional mKdV equation. The similarities using numerical analysis show that the exact answers are correct and faithful to the dynamics in terms of amplitude, width, phase evolution, and transmission speed. The steps used for testing make sure that the solutions are correct numerically, can be used with different types of analysis, and match what we would expect ion-acoustic structures to do in fractional plasma models.

2. The physical model of low-frequency ion-acoustic waves

In the present work, we examine the nonlinear dynamics of ion-acoustic waves in a magnetized, collisionless plasma system. The plasma under consideration is composed of singly charged inertial positive ions (with a charge e and a mass m_i) and two distinct populations of q-nonextensive electrons: A

population of cool electrons with the number density n_c, and a population of hot electrons with the number density n_h. At equilibrium, the quasi-neutrality condition is imposed as $n_{h0}/n_{i0}=1-q$, where the parameter $q=n_{c0}/n_{i0}$ denotes the ratio of the equilibrium cool electron density to ion density. The external magnetic field $\boldsymbol{B_0}$ is assumed to be aligned along the z-axis, i.e., $\boldsymbol{B_0}=B_0\,\underline{e}_z$, with $\underline{e}_z$ denoting the unit vector in the axial direction. The nonlinear evolution of ion-acoustic perturbations in such a plasma configuration is governed by a system of normalized fluid equations. These are generalized fractional versions of the continuity, momentum, and Poisson equations that include local interactions and strange transport phenomena.

The fractional continuity equation is a more general version of the standard continuity equation that includes the law of mass conservation. In fractional calculus, regular time or space derivatives are replaced by fractional-order operators. This lets us describe strange transport processes that cannot be described by integer-order dynamics. Mathematically, this equation may be expressed as

$$D_t^{\alpha} n_i + \nabla_{\alpha}(n_i \mathrm{u}) = 0, \quad \nabla_{\alpha} = D_x^{\alpha}\underline{e}_x + D_y^{\alpha}\underline{e}_y + D_z^{\alpha}\underline{e}_z, \quad \mathrm{u} = u\,\underline{e}_x + v\underline{e}_y + w\underline{e}_z. \tag{1}$$

Similarly, the fractional momentum equation constitutes a generalized form of the classical momentum equation of fluid or plasma dynamics. The addition of fractional derivatives lets the model show nonlocal and hereditary effects, as well as the strange transport processes that are often seen in complex plasma and viscoelastic media. The fractional momentum balance can be expressed as

$$D_t^{\alpha}\mathrm{u} + \mathrm{u}\nabla_{\alpha}\mathrm{u} + \nabla_{\alpha}\varphi + \mathrm{u}\times B_0\underline{e}_z = 0. \tag{2}$$

The fractional Poisson equation extends the standard electrostatic Poisson equation to include anomalous diffusion and nonlocal charge interactions. The standard form connects the divergence of the electric field to the charge density in the area, but the fractional formulation adds derivatives of noninteger order. This includes the effects of long-range correlations and fractal-like structures that are common in some plasma environments. This equation takes the form

$$\nabla_{\alpha}^2\varphi = \vartheta n_c + (1-\vartheta)n_h - n_i, \qquad \nabla_{\alpha}^2 = D_x^{\alpha\alpha} + D_y^{\alpha\alpha} + D_z^{\alpha\alpha}. \tag{3}$$

To model the electron populations, the number densities of the cool and hot electrons are assumed to follow the q-nonextensive distribution. This generalization improves the Maxwell–Boltzmann distribution by adding the nonextensive parameters q_c and q_h, which deal with long-range correlations and nonequilibrium phenomena. The corresponding distribution functions are given by

$$n_c = n_{c0}\left[1+\frac{e\varphi(q_c-1)}{k_B T_c}\right]^{\frac{q_c+1}{2(q_c-1)}}, \quad n_h = n_{h0}\left[1+\frac{e\varphi(q_h-1)}{k_B T_h}\right]^{\frac{q_h+1}{2(q_h-1)}}, \tag{4}$$

where n_{c0} and n_{h0} are the equilibrium densities that are not disturbed; T_c and T_h are the characteristic temperatures of the cool and hot electron species, respectively; e is the elementary charge; and φ is the electrostatic potential. The parameters q_c and q_h measure how nonextensive the cool and hot electron populations are, respectively.

It is important to note that in the limiting case where $q_c\to 1$ and $q_h\to 1$, the distribution reduces to the Maxwell–Boltzmann exponential form, thus adhering to the conventional thermodynamic equilibrium description. If q_c and q_h are both greater than 1, the distribution has superthermal tails that

are related to energetic electrons. When q_c and q_h are both less than 1, the distribution is cut off, which shows that high-energy states are being suppressed. This framework thus enables the modeling of a wide spectrum of nonequilibrium features observed in both space and astrophysical plasmas.

In this study, we restrict our analysis to the case $q_c,q_h<1$, a regime that is frequently employed in the investigation of superextensive plasma systems [23]. By applying a power series expansion of the exponential functions about zero, Eq (3) reduces to the following form:

$$D_x^{\alpha\alpha}\varphi + D_y^{\alpha\alpha}\varphi + D_z^{\alpha\alpha}\varphi = \mu_2\varphi^2 + \mu_1\varphi - n_i + 1, \tag{5}$$

where the coefficients μ_1 and μ_2 are determined by the two-temperature electron populations and the corresponding nonextensive parameters. Explicitly, these coefficients are expressed as

$$\begin{aligned} \mu_1 &= \frac{\vartheta(q_c+1)+(1-\vartheta)(q_h+1)\delta}{2}, \\ \mu_2 &= \frac{\vartheta(q_c+1)(3-q_c)+(1-\vartheta)(q_h+1)(3-q_h)\delta^2}{8}, \end{aligned} \tag{6}$$

where $\delta=T_h/T_c$ denotes the ratio of hot to cool electron temperatures. These expressions highlight the modifications to the nonlinear coefficients of plasma dynamics induced by deviations from the Maxwell–Boltzmann equilibrium (i.e., $q_c,\ q_h \neq 1$). For numerical analysis, we adopt representative parameter ranges: $q \in [0.1, 0.4]$, $\delta \in [0.1, 1]$, and $q_c,\ q_h \in [0.3, 1]$. These values are consistent with those commonly reported in both the laboratory and astrophysical plasma contexts, thereby ensuring the physical relevance of the present model. Finally, it should be emphasized that the results encapsulated in Eqs (1)–(6) reduce to and coincide with those previously reported in Ref. [23] when the fractional parameter is set to α = 1, thereby demonstrating the consistency of the proposed generalized framework with established classical plasma theory.

3. Derivation of the fractional space–time mKdV model

We use the RPM to look into how nonlinear waves move through the current plasma system. This asymptotic method is often used to make nonlinear wave equations easier to work with by taking advantage of the smallness of the waves' amplitude and systematically generating simplified evolution equations. The core of the strategy is to use a set of stretched coordinates for space and time that are properly calibrated to balance the effects of nonlinearity and dispersion. This rescaling changes the governing fluid and field equations into a simpler form that makes the slow spatiotemporal evolution of the waves stand out. These kinds of changes make it possible to find evolution equations (such the KdV and mKdV) that have solutions for solitary waves and shocks. This method not only explains how waves get steeper and spread out, but it also shows how solitary structures in dusty plasmas behave, where nonlinear and dispersive processes naturally happen at the same time. The extended coordinates for space and time are introduced as follows, using the typical reductive perturbation scheme:

$$\xi = \frac{\varepsilon}{\alpha}\left(k_1 x^{\alpha} + k_2 y^{\alpha} + k_3 z^{\alpha} - \alpha V\, t^{\alpha}\right), \qquad \tau = \frac{\varepsilon^3}{\alpha} t^{\alpha}. \tag{7}$$

In this context, V signifies the phase velocity of the ion-acoustic waves, whereas ϵ denotes a minor perturbation parameter that defines the waves' amplitude. The parameters k_1, k_2, and k_3 are the cosines of the wave vector's direction along the x-, y-, and z-axes, respectively. This is true as long as $k_1^2 + k_2^2 + k_3^2 = 1$. The fractional operator applied to a scalar field is represented as a convolution of the field with a suitable kernel, thus integrating the influences of nonlocal interactions. This expanded formulation gives a more complete picture of how waves move across difficult media. Dispersion and damping effects are examples of the sorts of physical phenomena that are commonly ignored in conventional integer-order systems. This method takes these types of things into account. Adding fractional calculus to the analysis makes modeling wave function better, which makes the system more accurate and better at making predictions, especially in systems that demonstrate strange transport phenomena. This new way of thinking not only helps us understand how waves function better, but it also opens up new doors for technology. To be able to create complex materials that possess certain characteristics, it is necessary to have the ability to forecast how waves will behave in various locations and to use wave optimization techniques in order to do this. Specifically, this is of the greatest importance for the industrial sector of the economy. Changes of this kind might result in the development of new technologies that have the potential to revolutionize the functioning of a wide range of industries, including, but not limited to, photonics, energy storage systems, and telecommunications, to mention just a few. It is expected that the continued advancement of fractional models will offer new possibilities to combine theoretical plasma physics with real-world applications in contemporary engineering and materials science as research in this field continues to advance. Within the confines of this paradigm, the fractional operator that functions on a scalar field may be written as

$$\begin{aligned} &D_x^{\alpha} = k_1 \varepsilon D_{\xi}^{\alpha}, \quad D_x^{\alpha\alpha} = k_1^2 \varepsilon^2 D_{\xi}^{\alpha\alpha}, \quad D_y^{\alpha} = k_2 \varepsilon D_{\xi}^{\alpha}, \quad D_y^{\alpha\alpha} = k_2^2 \varepsilon^2 D_{\xi}^{\alpha\alpha}, \\ &D_z^{\alpha} = k_3 \varepsilon D_{\xi}^{\alpha}, \quad D_z^{\alpha\alpha} = k_3^2 \varepsilon^2 D_{\xi}^{\alpha\alpha}, \qquad D_t^{\alpha} = -\alpha V \varepsilon D_{\xi}^{\alpha} + \varepsilon^3 D_{\tau}^{\alpha}. \end{aligned} \tag{8}$$

The CFD is used in this study because it allows a consistent extension of traditional analytical methods to the fractional domain while preserving the important features of classical integer-order differentiation, such as the product rule and chain rule, and handling implicit functions. For instance, the operators appearing in Eq (8) can be computed directly using the CFD's definition, since $\frac{\partial^{\alpha}}{\partial x^{\alpha}} = \frac{\partial^{\alpha}\xi}{\partial x^{\alpha}} \frac{\partial^{\alpha}}{\partial \xi^{\alpha}}$ which gives $D_x^{\alpha} = k_1 \varepsilon D_{\xi}^{\alpha}$, and analogous expressions hold for the remaining operators. This allows the reductive perturbation framework to be applied without introducing nonlocal integral kernels. Moreover, the CFD is defined for both differentiable and nondifferentiable functions, making it suitable for modeling continuous as well as noncontinuous media (see Refs. [47–50]). We stress that the CFD is a local operator and does not store true long-range memory in the strict meaning of hereditary integral formulations, unlike the Caputo or Riemann–Liouville derivatives. Hence, in this plasma model, the CFD does not reflect complete nonlocal memory but rather effects a fractional distortion of the local nonlinear–dispersive balance by means of power-law scaling of both space and time.

To clarify the physical interpretation of the CFD within the present plasma framework, we emphasize that the CFD acts as a local fractional scaling operator rather than a hereditary memory operator. In contrast to the Caputo, Riemann–Liouville, or Atangana–Baleanu derivatives, which incorporate nonlocal convolution kernels and therefore encode long-range temporal memory, the CFD modifies the evolution of the plasma variables through a local power-law scaling of spatial and

temporal gradients. This fractional rescaling, expressed in the form $D^{\beta}\psi(\varphi)=\frac{d\psi}{d\varphi}D^{\beta}\varphi$, and $D^{\beta}\varphi(x)=x^{1-\beta}\frac{d\varphi}{dx}$, provides a phenomenological mechanism to represent anomalous transport, weak collisionality, intermittency, or non-Maxwellian effects that alter the effective balance between nonlinearity and dispersion. Because the CFD preserves the classical product, chain, and composition rules, it allows the RPM and Hirota bilinear formulation to extend consistently into the fractional domain without introducing nonlocal integral operators. Thus, in the present model, the fractional order α should be understood as a continuous parameter that modulates the nonlinear–dispersive structure of ion-acoustic waves through local fractional scaling (rather than through true long-range memory) and thereby provides a controlled way to explore departures from the classical mKdV dynamics in complex plasma environments.

By substituting the stretched operators defined in Eq (8) into the governing Eqs (1), (2), and (5), we obtain their transformed forms in terms of the stretched variables ξ and τ, and the factor ε as

$$-\alpha V\ D_{\xi}^{\alpha}n_i+\varepsilon^2 D_{\tau}^{\alpha}n_i+k_1 D_{\xi}^{\alpha}(n_i u)+k_2 D_{\xi}^{\alpha}(n_i v)+k_3 D_{\xi}^{\alpha}(n_i w)=0. \tag{9}$$

If we apply these to each component of Eq (2) and factor out ε, the *x*-component is

$$-\alpha V\ \varepsilon D_{\xi}^{\alpha}u+\varepsilon^3 D_{\tau}^{\alpha}u+k_1\varepsilon u\, D_{\xi}^{\alpha}u+k_2\varepsilon v\, D_{\xi}^{\alpha}u+k_3\varepsilon w\, D_{\xi}^{\alpha}u+k_1\varepsilon D_{\xi}^{\alpha}\varphi-\sqrt{\varepsilon}B_0 v=0, \tag{10}$$

The *y*-component is

$$-\alpha V\ \varepsilon D_{\xi}^{\alpha}v+\varepsilon^3 D_{\tau}^{\alpha}v+k_1\varepsilon u\, D_{\xi}^{\alpha}v+k_2\varepsilon v\, D_{\xi}^{\alpha}v+k_3\varepsilon w D_{\xi}^{\alpha}v+k_2\varepsilon D_{\xi}^{\alpha}\varphi+\sqrt{\varepsilon}B_0 u=0, \tag{11}$$

The *z*-component is

$$-\alpha V D_{\xi}^{\alpha}w+\varepsilon^2 D_{\tau}^{\alpha}w+k_1 u\, D_{\xi}^{\alpha}w+k_2 v\, D_{\xi}^{\alpha}w+k_3 w D_{\xi}^{\alpha}w+k_2 D_{\xi}^{\alpha}\varphi=0. \tag{12}$$

Equation (5) becomes

$$\varepsilon^2(k_1^2+k_2^2+k_3^2)D_{\xi}^{\alpha\alpha}\varphi=\mu_2\varphi^2+\mu_1\varphi-n_i+1. \tag{13}$$

The dependent variables n_i, *u, v, w*, and φ are expanded as regular perturbation series in the small parameter ε as

$$\begin{aligned}
&n_i=1+\sqrt{\varepsilon}n_{i1}+\varepsilon n_{i2}+\sqrt{\varepsilon^3}n_{i3}+\ldots,\ u=0+\varepsilon u_1+\sqrt{\varepsilon^3}u_2+\varepsilon^2 u_3+\ldots,\\
&v=0+\varepsilon v_1+\sqrt{\varepsilon^3}v_2+\varepsilon^2 v_3+\ldots,\quad w=0+\sqrt{\varepsilon}w_1+\varepsilon w_2+\sqrt{\varepsilon^3}w_3+\ldots,\\
&\varphi=0+\varphi_1\sqrt{\varepsilon}+\varphi_2\varepsilon+\varphi_3\sqrt{\varepsilon^3}+\ldots.
\end{aligned} \tag{14}$$

Using Eq (14) in Eqs (9)–(13), and collecting the terms of ε in the lowest order from Eq (9), one can obtain

$$-\alpha V\ D_{\xi}^{\alpha}(1+\sqrt{\varepsilon}n_{i1}+\varepsilon n_{i2}+\sqrt{\varepsilon^3}n_{i3}+...)+\varepsilon^2 D_{\tau}^{\alpha}(1+\sqrt{\varepsilon}n_{i1}+\varepsilon n_{i2}+\sqrt{\varepsilon^3}n_{i3}+...)+k_1 D_{\xi}^{\alpha}((1+\sqrt{\varepsilon}n_{i1}$$
$$+\varepsilon n_{i2}+\sqrt{\varepsilon^3}n_{i3}+...)(\varepsilon u_1+\sqrt{\varepsilon^3}u_2+\varepsilon^2 u_3+...))+k_2 D_{\xi}^{\alpha}((1+\sqrt{\varepsilon}n_{i1}+\varepsilon n_{i2}+\sqrt{\varepsilon^3}n_{i3}+...)(\varepsilon v_1+\sqrt{\varepsilon^3}v_2$$
$$+\varepsilon^2 v_3+...))+k_3 D_{\xi}^{\alpha}((1+\sqrt{\varepsilon}n_{i1}+\varepsilon n_{i2}+\sqrt{\varepsilon^3}n_{i3}+...)(\sqrt{\varepsilon}w_1+\varepsilon w_2+\sqrt{\varepsilon^3}w_3+...))=0.$$
$$\sqrt{\varepsilon}:\quad -\alpha V\ D_{\xi}^{\alpha}n_{i1}+k_3 D_{\xi}^{\alpha}w_1=0,$$
$$\varepsilon:\quad -\alpha V\ D_{\xi}^{\alpha}n_{i2}+k_1 D_{\xi}^{\alpha}u_1+k_2 D_{\xi}^{\alpha}v_1+k_3 D_{\xi}^{\alpha}w_2+k_3 D_{\xi}^{\alpha}(n_{i1}w_1)=0,$$
$$\sqrt{\varepsilon^3}:-\alpha V\ D_{\xi}^{\alpha}n_{i3}+k_1 D_{\xi}^{\alpha}u_2+k_2 D_{\xi}^{\alpha}v_2+k_3 D_{\xi}^{\alpha}w_3+k_1 D_{\xi}^{\alpha}(n_{i1}u_1)+k_2 D_{\xi}^{\alpha}(n_{i1}v_1)+k_3 D_{\xi}^{\alpha}(n_{i1}w_2)=0.$$

From Eq (10), one can obtain

$$-\alpha V\ \varepsilon D_{\xi}^{\alpha}(\varepsilon u_1+\sqrt{\varepsilon^3}u_2+\varepsilon^2 u_3+...)+\varepsilon^3 D_{\tau}^{\alpha}(\varepsilon u_1+\sqrt{\varepsilon^3}u_2+\varepsilon^2 u_3+...)+k_1\varepsilon(\varepsilon u_1+\sqrt{\varepsilon^3}u_2+\varepsilon^2 u_3+...)D_{\xi}^{\alpha}(\varepsilon u_1$$
$$+\sqrt{\varepsilon^3}u_2+\varepsilon^2 u_3+...)+k_2\varepsilon(\varepsilon v_1+\sqrt{\varepsilon^3}v_2+\varepsilon^2 v_3+...)D_{\xi}^{\alpha}(\varepsilon u_1+\sqrt{\varepsilon^3}u_2+\varepsilon^2 u_3+...)+k_3\varepsilon(\sqrt{\varepsilon}w_1+\varepsilon w_2+\sqrt{\varepsilon^3}w_3$$
$$+...)D_{\xi}^{\alpha}(\varepsilon u_1+\sqrt{\varepsilon^3}u_2+\varepsilon^2 u_3+...)+k_1\varepsilon D_{\xi}^{\alpha}(\varphi_1\sqrt{\varepsilon}+\varphi_2\varepsilon+\varphi_3\sqrt{\varepsilon^3}+...)-\sqrt{\varepsilon}B_0(\varepsilon v_1+\sqrt{\varepsilon^3}v_2+\varepsilon^2 v_3+...)=0,$$
$$\sqrt{\varepsilon^3}:\quad k_1 D_{\xi}^{\alpha}\varphi_1-B_0 v_1=0,$$
$$\varepsilon^2:\quad -\alpha V D_{\xi}^{\alpha}u_1+k_1 D_{\xi}^{\alpha}\varphi_2-B_0 v_2=0.$$

From Eq (11), one can obtain

$$-\alpha V\ \varepsilon D_{\xi}^{\alpha}(\varepsilon v_1+\sqrt{\varepsilon^3}v_2+\varepsilon^2 v_3+...)+\varepsilon^3 D_{\tau}^{\alpha}(\varepsilon v_1+\sqrt{\varepsilon^3}v_2+\varepsilon^2 v_3+...)+k_1\varepsilon(\varepsilon u_1+\sqrt{\varepsilon^3}u_2+\varepsilon^2 u_3+...)$$
$$D_{\xi}^{\alpha}(\varepsilon v_1+\sqrt{\varepsilon^3}v_2+\varepsilon^2 v_3+...)+k_2\varepsilon(\varepsilon v_1+\sqrt{\varepsilon^3}v_2+\varepsilon^2 v_3+...)D_{\xi}^{\alpha}(\varepsilon v_1+\sqrt{\varepsilon^3}v_2+\varepsilon^2 v_3+...)+k_3\varepsilon(\sqrt{\varepsilon}w_1$$
$$+\varepsilon w_2+\sqrt{\varepsilon^3}w_3+...)D_{\xi}^{\alpha}(\varepsilon v_1+\sqrt{\varepsilon^3}v_2+\varepsilon^2 v_3+...)+k_2\varepsilon D_{\xi}^{\alpha}(\varphi_1\sqrt{\varepsilon}+\varphi_2\varepsilon+\varphi_3\sqrt{\varepsilon^3}+...)$$
$$+\sqrt{\varepsilon}B_0(\varepsilon u_1+\sqrt{\varepsilon^3}u_2+\varepsilon^2 u_3+...)=0,$$
$$\sqrt{\varepsilon^3}:\quad k_2 D_{\xi}^{\alpha}\varphi_1+B_0 u_1=0,$$
$$\varepsilon^2:\quad -\alpha V D_{\xi}^{\alpha}v_1+k_2 D_{\xi}^{\alpha}\varphi_2+B_0 u_2=0.$$

From Eq (12), one can obtain

$$-\alpha V D_{\xi}^{\alpha}(\sqrt{\varepsilon}w_1+\varepsilon w_2+\sqrt{\varepsilon^3}w_3+...)+\varepsilon^2 D_{\tau}^{\alpha}(\sqrt{\varepsilon}w_1+\varepsilon w_2+\sqrt{\varepsilon^3}w_3+...)+k_1(\varepsilon u_1+\sqrt{\varepsilon^3}u_2+\varepsilon^2 u_3+...)$$
$$D_{\xi}^{\alpha}(\sqrt{\varepsilon}w_1+\varepsilon w_2+\sqrt{\varepsilon^3}w_3+...)+k_2(\varepsilon v_1+\sqrt{\varepsilon^3}v_2+\varepsilon^2 v_3+...)D_{\xi}^{\alpha}(\sqrt{\varepsilon}w_1+\varepsilon w_2+\sqrt{\varepsilon^3}w_3+...)$$
$$+k_3(\sqrt{\varepsilon}w_1+\varepsilon w_2+\sqrt{\varepsilon^3}w_3+...)D_{\xi}^{\alpha}(\sqrt{\varepsilon}w_1+\varepsilon w_2+\sqrt{\varepsilon^3}w_3+...)+k_2 D_{\xi}^{\alpha}(\varphi_1\sqrt{\varepsilon}+\varphi_2\varepsilon+\varphi_3\sqrt{\varepsilon^3}+...)=0,$$
$$\sqrt{\varepsilon}:\quad -\alpha V D_{\xi}^{\alpha}w_1+k_2 D_{\xi}^{\alpha}\varphi_1=0,$$
$$\varepsilon:\quad -\alpha V D_{\xi}^{\alpha}w_2+k_3 w_1 D_{\xi}^{\alpha}w_1+k_2 D_{\xi}^{\alpha}\varphi_2=0.$$

From Eq (13), one can obtain

$$\varepsilon^2(k_1^2+k_2^2+k_3^2)D_\xi^{\alpha\alpha}(\varphi_1\sqrt{\varepsilon}+\varphi_2\varepsilon+\varphi_3\sqrt{\varepsilon^3}+\ldots)=\mu_2(\varphi_1\sqrt{\varepsilon}+\varphi_2\varepsilon+\varphi_3\sqrt{\varepsilon^3}+\ldots)^2+\mu_1(\varphi_1\sqrt{\varepsilon}+\varphi_2\varepsilon$$
$$+\varphi_3\sqrt{\varepsilon^3}+\ldots)-(1+\sqrt{\varepsilon}n_{i1}+\varepsilon n_{i2}+\sqrt{\varepsilon^3}n_{i3}+\ldots)+1.$$

$$\sqrt{\varepsilon}: \qquad \mu_1\varphi_1-n_{i1}=0,$$
$$\varepsilon: \qquad \mu_2\varphi_1+\mu_1\varphi_2-n_{i2}=0.$$

We use the conformable fractional integration and using the boundary conditions

$$n_{i1}=0, \quad u_1=0, \quad v_1=0, \quad w_1=0, \quad \varphi_1=0 \quad \text{at} \quad \xi\to\infty,$$

to obtain the first-order perturbed quantities listed below:

$$n_1=\frac{k_3^2\varphi_1}{\alpha^2V^2}, \quad u_1=-\frac{k_2}{B_0}D_\xi^\alpha\varphi_1, \quad v_1=\frac{k_1}{B_0}D_\xi^\alpha\varphi_1, \quad w_1=\frac{k_3\varphi_1}{\alpha V}, \quad V^2=\frac{k_3^2}{\alpha^2\mu_1}, \tag{15}$$

in the same manner, we obtain

$$\begin{aligned} &n_2=\mu_2\varphi_1^2-\frac{\mu_1k_3^2\varphi_1^2}{2\alpha^2V^2}, \quad u_2=\frac{1}{\alpha^2V^2B_0^2}\left(k_2k_3^2B_0D_\xi^\alpha\varphi_1+\alpha^3V^3k_1D_\xi^{\alpha\alpha}\varphi_1\right),\\ &v_2=\frac{1}{\alpha^2V^2B_0^2}\left(-k_1k_3^2B_0\varphi_1D_\xi^\alpha\varphi_1+\alpha^3V^3k_2D_\xi^{\alpha\alpha}\varphi_1\right), \quad w_2=0, \quad \varphi_2=-\frac{k_3^2\varphi_1^2}{2\alpha^2V^2}. \end{aligned} \tag{16}$$

As we move on to the next order in ϵ, we get more correction terms that make the model's analytical framework better. This higher-order expansion allows for a more accurate description of the system's nonlinear behavior and gives us a better understanding of the processes that drive its change.

$$\begin{aligned} &k_2D_\xi^\alpha(n_1v_1)+k_3D_\xi^\alpha(n_1w_2)+k_1D_\xi^\alpha(n_1u_1)+k_3D_\xi^\alpha(n_2w_1)+k_1n_1D_\xi^\alpha u_1+k_2n_1D_\xi^\alpha v_1\\ &+k_3n_2D_\xi^\alpha w_1-\alpha V D_\xi^\alpha n_3+k_1D_\xi^\alpha u_2+k_2D_\xi^\alpha v_2+k_3D_\xi^\alpha w_3+D_\tau^\alpha n_1=0. \end{aligned} \tag{17}$$

By merging Eqs (15)–(17) and establishing $\varphi=\varphi_1$, we derive the space–time fractional mKdV equation

$$D_\tau^\alpha\varphi+A\,\varphi^2D_\xi^\alpha\varphi+B\,D_\xi^{\alpha\alpha\alpha}\varphi=0. \tag{18}$$

with the nonlinearity and dispersion coefficients, respectively, defined by

$$A=\frac{2\alpha^4\mu_2V^4+3k_3^4}{2\alpha^3V^3}, \tag{19}$$

$$B=\frac{\alpha^3V^3(k_1^2+k_2^2)}{B_0^2k_3^2}. \tag{20}$$

In addition to providing a solid foundation for investigating soliton solutions, this governing equation provides a concise summary of the most significant aspects of the nonlinear dynamics that are

being investigated. The appearance of the space–time fractional mKdV equation is especially intriguing because it sheds insight on the delicate equilibrium that exists between nonlinearity and dispersion, which is what makes it possible for localized wave structures to be formed and to remain stable. As a result of an in-depth investigation of the space–time fractional mKdV equation, it is feasible to get further knowledge on ion-acoustic solitons in plasma systems. This work is also linked to other areas of physics, like nonlinear optics and fluid dynamics. Soliton solutions are a key way to learn about how nonlinear waves behave, interact, and stay stable over time in complex media. As these new ideas grow, theoretical models get better. This means that they can predict a wider range of physical events. This cycle will keep going until everyone fully understands the new ideas. It is important for more than just plasma physics to understand the soliton hypothesis. This idea is very important. In addition to this, it demonstrates that it is of the highest relevance in a wide range of scientific and technological disciplines, particularly those that need the precise management of wave dynamics. For the sake of illustration, some instances that are particularly noteworthy are developments in the field of materials engineering, optical communication systems, and technology for the transfer of energy. It is envisaged that new connections between many disciplines of research will establish themselves as the exploration of the space–time fractional mKdV equation and the soliton solutions related to it continues to make progress. It is expected that the relationship between theoretical mathematical abstraction and practical investigation would be strengthened as a result of these discoveries. In addition to this, the findings that are made will shed light on the significant connection that takes place between nonlinear mathematics and actual physical systems. It is possible that the development of these enhancements will make it possible to create fresh applications in the sectors of technology and engineering, which are becoming more relevant due to the fact that understanding of nonlinear wave phenomena is becoming more prevalent.

For reproducibility, we summarize the specific assumptions underlying the space–time fractional mKdV formulation. (i) The plasma consists of a warm ion population and two electron species (cold/thermal and hot) in a uniform background magnetic field, with all equilibrium quantities being spatially uniform. (ii) Perturbations are assumed to be weak and slowly varying, enabling the RPM in the stretched variables $\xi = \varepsilon\left(k_1 x^{\alpha} + k_2 y^{\alpha} + k_3 z^{\alpha} - \alpha V\, t^{\alpha}\right)/\alpha$ and $\tau = \varepsilon^3 t^{\alpha}/\alpha$, where $\epsilon \ll 1$. (iii) The CFD is adopted as a local generalization of the classical derivative, with the standard product and chain rules being preserved, ensuring that the RPM and Hirota bilinear techniques remain mathematically consistent. (iv) Only right-propagating, long-wavelength ion-acoustic modes are retained; higher order dispersion, strong damping, and finite Larmor radius effects are neglected. (v) The integration constants in the traveling wave reduction are chosen to eliminate nonphysical mean drifts, following standard mKdV analyses. (vi) For all soliton and periodic solutions, the wave number k and frequency ω satisfy the fractional dispersion relation derived from the bilinear formalism, and all parameters (A,B,α,k,ω) are specified explicitly to enable direct numerical or symbolic reproduction. These assumptions ensure that each analytical solution (solitary, kink, periodic, or multi-soliton) is uniquely determined and reproducible under the same parameter settings.

4. Existence of traveling wave solutions

The space–time fractional mKdV model is very important for explaining how ion-acoustic waves move in magnetized plasmas in a nonlinear way. In this part, we use suitable transformations and solution methods to clarify the analytical solutions of the model. Using this method, we find solitary

wave, kink-type, and periodic solutions that help us understand how the system works on its own. These precise answers enhance our comprehension of the interaction between dispersion and nonlinearity in waves' evolution, while also functioning as essential benchmarks for the validation of numerical methods and the analysis of more intricate plasma models.

We specifically demonstrate the existence of traveling wave solutions for the space–time fractional mKdV equation. Using a typical traveling wave transformation, the governing system is simplified to an ordinary differential system in the phase plane. By looking at the equilibrium points, which tell us what kinds of trajectories are possible in the phase space, we can then figure out how the reduced system behaves qualitatively. Using the qualitative theory of dynamic systems, we find the conditions that allow for the existence of heteroclinic, homoclinic, and periodic orbits. These orbits correspond to kink/antikink waves, solitary waves, and periodic wave solutions of the original fractional mKdV model.

The classification of these waveforms is articulated by the governing parameters A and B, which directly affect both the existence and the qualitative characteristics of the moving waves. To investigate the presence of traveling wave solutions for the space–time fractional mKdV model, we present the typical traveling wave transformation as follows:

$$\varphi(\xi,\tau)=\varphi(\zeta), \qquad \zeta=\frac{1}{\alpha}(k\,\xi^{\alpha}-\alpha\omega\,\tau^{\alpha}), \tag{21}$$

where $\varphi(\zeta)$ represents the shape of the wave, and k and ω denote the wave number and wave velocity, respectively. Let $\varphi(\zeta)$ be a continuous solution of Eq (18) satisfying

$$\lim_{\zeta\to\pm\infty}\varphi(\zeta)=\rho^{\pm}. \tag{22}$$

Then $\varphi(\zeta)$ is called a kink/antikink solution if $\rho^{+}\neq\rho^{-}$, and $\phi(\xi)$ is called a solitary (bright or dark**)** solution if $\rho^{+}=\rho^{-}$. By utilizing the traveling wave transformation (21) in the space–time fractional mKdV of Eq (18) and applying the property $D_{\xi}^{\alpha}\varphi(\zeta)=\frac{d\varphi}{d\zeta}D_{\xi}^{\alpha}\varphi$, we have $D_{\tau}^{\alpha}\varphi=-\alpha\omega\varphi'$, $D_{\xi}^{\alpha}\varphi=k\,\varphi'$, and $D_{\xi}^{\alpha\alpha\alpha}\varphi=k^{3}\varphi'''$. We derive the following ODE:

$$-\alpha\,\omega\varphi'+kA\,\varphi^{2}\,\varphi'+k^{3}B\,\varphi'''=0, \tag{23}$$

Integrating Eq (23) with respect to ζ and setting the integration constant to zero yields

$$-\alpha\,\omega\varphi+\frac{kA}{3}\varphi^{3}+k^{3}B\,\varphi''=0,$$

which can be written equivalently as

$$\varphi''=\rho_{1}\varphi+\rho_{2}\varphi^{3}, \tag{24}$$

where $\rho_{1}=\frac{\alpha\,\omega}{k^{3}B}$, $\rho_{2}=-\frac{A}{3k^{2}B}$. Equation (24) can be written in the following system:

$$\begin{aligned} \frac{d\varphi}{d\zeta} &= \psi, \\ \frac{d\psi}{d\zeta} &= \frac{\alpha\omega}{k^3 B}\varphi - \frac{A}{3k^2 B}\varphi^3. \end{aligned} \tag{25}$$

Solitary wave solutions correspond to homoclinic orbits, shock structures are associated with heteroclinic connections, and periodic wave solutions arise from closed orbits in the phase plane. By expressing Eq (24) in the traveling wave form $\varphi'' = F(\varphi)$, and introducing the appropriate reduction $\varphi' = \psi$, the system can be reformulated in Hamiltonian form. Setting the corresponding parameters, the Hamiltonian associated with the reduced system is obtained as follows:

$$H(\varphi,\psi) = \frac{1}{2}\psi^2 + U(\varphi), \qquad U(\varphi) = -\int^{\varphi} F(s)ds,$$

which is conserved along trajectories. Homoclinic orbits occur at the saddle energy level $H=H_s$, periodic orbits for energies occur between neighboring extrema of U, and heteroclinic (shock) connections link distinct asymptotic states $\varphi_{\pm}$ with equal energy $U(\varphi_+)=U(\varphi_-)$.

$$H(\varphi,\psi) = \psi^2 - \frac{\alpha\omega}{k^3 B}\varphi^2 + \frac{A}{6k^2 B}\varphi^4 = h. \tag{26}$$

To provide a rigorous confirmation of the qualitative phase portrait classification, we supplement the discussion with an explicit eigenvalue analysis of the equilibrium points of system (25). Linearizing the system

$$\varphi' = \psi, \qquad \psi' = \frac{1}{3k^3 B}(3\alpha\omega\varphi - kA\varphi^3),$$

around an equilibrium point $E=(\varphi_e,0)$ yields the Jacobian matrix

$$J(E) = \begin{pmatrix} 0 & 1 \\ \frac{1}{3k^3 B}(3\alpha\omega - kA\varphi^2) & 0 \end{pmatrix}.$$

The corresponding eigenvalues satisfy

$$\lambda^2 = \frac{1}{3k^3 B}(3\alpha\omega - kA\varphi^2). \tag{27}$$

Since $A > 0$, $B > 0$, the sign of $(3\alpha\omega - kA\varphi^2)/3k^3 B$ determines the nature of the equilibrium. This leads to the following distinct cases. (1) If $\omega < 0$ and $k < 0$, the origin $E_1(0,0)$ acts as a center, while two saddle points emerge at $E_2\left(\sqrt{3\alpha\omega/Ak},0\right)$ and $E_3\left(-\sqrt{3\alpha\omega/Ak},0\right)$. In this configuration, closed periodic orbits form around the center, and the saddle points are connected by separatrices that delineate the boundary of these periodic trajectories. (2) If $\omega < 0$ and $k > 0$, the origin $E_1(0,0)$ is the sole equilibrium point and functions as a center. In this scenario, the phase portrait is dominated by closed periodic orbits encircling the center, indicating stable oscillatory motion. (3) If $\omega > 0$ and $k < 0$, only the origin $E_1(0,0)$ exists and behaves as a saddle point. Trajectories either diverge away from or

converge toward the origin along its unstable and stable manifolds, respectively. (4) If $\omega > 0$ and $k > 0$, the origin $E_1(0,0)$ becomes a saddle point, while two centers appear at $E_2\left(\sqrt{3\alpha\omega / A\,k}\,,0\right)$ and $E_3\left(-\sqrt{3\alpha\omega / A\,k}\,,0\right)$. The saddle point is connected to itself by homoclinic separatrices, which form closed curves enclosing the two centers. Figure 1 illustrates these four configurations at A=1, B=1, and α= 1: (a) When ω= –1 and k = –1, (b) when k = 1 and ω = –1, (c) when k = –1 and ω = *1*, (d) when k = 1 and ω = 1. The classification above elucidates the manner in which the interplay between the parameters k and ω determines both the quantity and the stability characteristics of the equilibrium points. If $k\,\omega < 0$, the system has only one equilibrium point at the origin. Linearizing it gives either a center (which is neutrally stable in the Hamiltonian sense) or a saddle (which is unstable). The global dynamics are correspondingly simple, with closed periodic trajectories or trajectories that leave along saddle manifolds. In contrast, when $k\,\omega > 0$, three equilibria emerge, and the phase portrait exhibits an enhanced structure: Separatrices (the stable and unstable manifolds of saddle points and, where relevant, homoclinic connections) divide the phase plane into invariant regions, thereby restricting the trajectories to the designated domains. This coexistence of stable (center) and unstable (saddle) structures is typical of nonlinear Hamiltonian flows.

In the example of Case 1, separatrix geometry arranges the phase space so that periodic orbits around the central equilibrium are separate from the motion outside of it. There are homoclinic separatrices around the centers that come from the saddle in Case 4. These separatrices prevent trajectories that are close to the centers from moving through them, but they let them move freely outside of them. Bifurcations are the name given to these alterations in the topology of the phase portrait that are brought about by parameters. They provide evidence that the behavior of the system has undergone significant changes. One of the most essential things that has to be done is to locate and categorize these bifurcations. This will allow us to accurately forecast how even small adjustments to the parameters might result in significant changes in behavior. The insights that were acquired in the domains of physics and biology, where dynamic systems approaches are used to assist in finding stability zones, the beginning of complex or chaotic processes, and the creation of effective control or intervention strategies are generally useful across a number of other sectors. It is possible that a systematic bifurcation analysis might significantly increase our theoretical knowledge and make it much simpler to make judgments in domains such as engineering, ecology, and economics, amongst others, which need extremely precise forecasts of how systems would act. This is very important, since the professionals in these fields need to be able to make precise forecasts on the functioning of the systems.

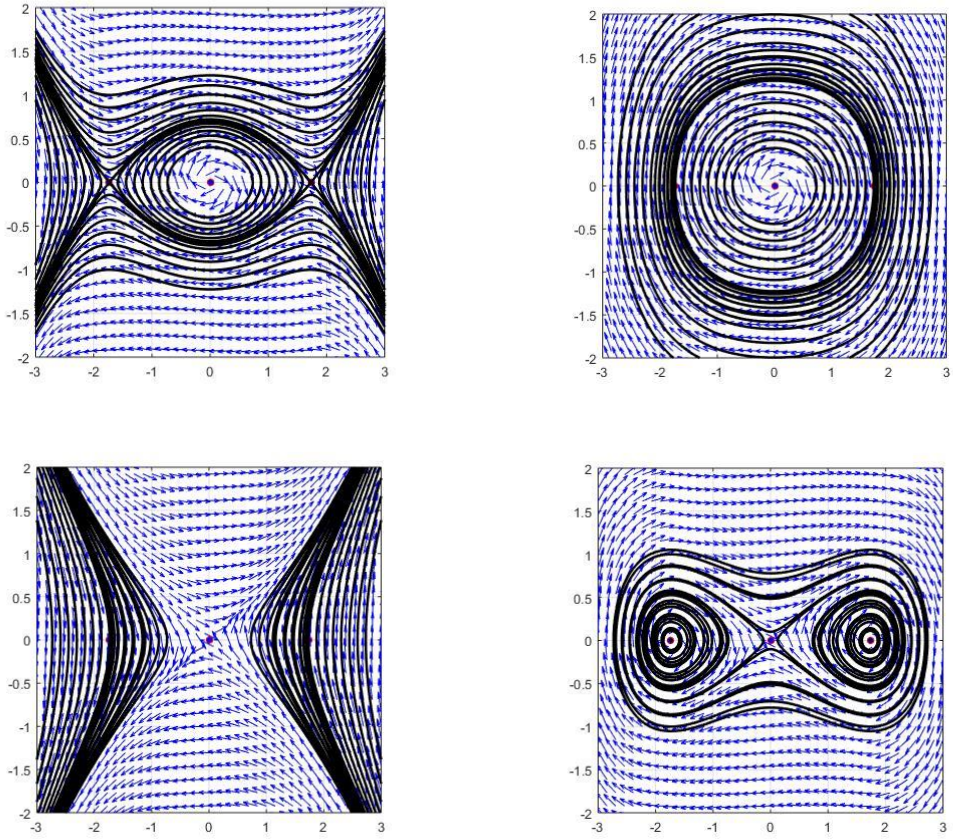

Figure 1. Phase portraits of the dynamic system (25) at $A = 1$, $B = 1$, and $\alpha = 1$ for different parameter regimes. (a) $\omega = -1$ and $k = -1$: A center at the origin with saddles connected by separatrices. (b) $k = 1$, $\omega = -1$: A single center at the origin with periodic closed orbits. (c) $k = -1$, $\omega = 1$: A single saddle point at the origin with diverging/converging trajectories. (d) $k = 1$, $\omega = 1$: A saddle point at the origin with two centers enclosed by homoclinic separatrices. These configurations highlight the relationship between the parameters v and μ and the existence of periodic, solitary, and kink-type traveling wave solutions.

The link between the phase portraits of System (25) and the physical waveforms of the fractional mKdV equation follows directly from reduction of the traveling wave. System (25) admits the Hamiltonian Eq (26). Solitary, periodic, and kink waves correspond to distinct energy levels in the potential $U(\varphi)$. Solitary waves (homoclinic orbits) occur when $H = U(\varphi_s)$, which is the saddle energy level. The trajectory leaves the saddle and returns to it: $\varphi(\xi) \to \varphi_s$ as $|\xi| \to \infty$. The resulting waveform satisfies $\varphi(-\infty) = \varphi(\infty) = \varphi_s$, which is the defining property of a solitary pulse. This yields the sech-type soliton profiles obtained analytically. Kink/antikink waves (heteroclinic orbits) occur when the trajectory connects two distinct equilibria, namely $\varphi(-\infty) = \varphi_-$, $\varphi(\infty) = \varphi_+$, with $U(\varphi_-) = U(\varphi_+) = H$. The sign of $k\omega$ determines whether the two nonzero equilibria exist. This gives the tanh-type kink and antikink solutions derived explicitly. Periodic waves (closed orbits) occur for energy levels strictly between two turning points of the potential: $U_{min} < H < U_{max}$. The closed orbit corresponds to a periodic oscillation of $\varphi(\xi)$ between two symmetric turning points. This yields the Jacobi elliptic cn/sn/dn periodic solutions. Thus, the classification of solitary, kink-type, and periodic waves follows rigorously from

the Hamiltonian formulation and the energy-level structure of the reduced dynamic system, not from qualitative analogy.

4.1. Chaotic behavior under periodic perturbation

In the unperturbed case, reduction of the traveling wave leads to the two-dimensional autonomous system in (25). As a planar autonomous flow with a conserved Hamiltonian, the Poincaré–Bendixson theorem ensures that the dynamics consist exclusively of equilibria, periodic orbits, separatrices, and homoclinic/heteroclinic connections. Chaos is therefore impossible in the unperturbed system, and this is consistent with the regular phase portraits displayed in Figure 1. The situation changes once a periodic perturbation is introduced. The perturbed model can be expressed abstractly as

$$\begin{aligned} \frac{d\varphi}{d\zeta} &= \psi, \\ \frac{d\psi}{d\zeta} &= \frac{\alpha\omega}{k^3 B}\varphi - \frac{A}{3k^2 B}\varphi^3 + R(\Omega). \end{aligned} \tag{28}$$

In the perturbation term $R(\Omega)$, the variable Ω plays the role of a phase that evolves in time. In particular, the value of Ω may be expressed as a linear function of time, which can be expressed as $\Omega = \omega\,\mu + \varphi_0$, where ω represents the angular frequency that is associated with the system's intrinsic oscillations or external effects, and φ_0 represents an initial phase offset. As a result of this link, it can be deduced that the value of Ω increases in a time-dependent manner, and it also serves as a good foundation for periodic functions, which may be represented by the trigonometric perturbation $R(\Omega) = 0.5\cos(2\Omega)$. For this reason, the term "perturbation" is used to denote a force that is time-periodic and has a frequency that is multiplied by the factor $2\times\omega$. As can be seen in the corresponding phase images in Figure 2, this periodic modulation has an effect on the nonlinear dynamics of the system, which often leads to complex behaviors such as quasi-periodicity and chaos.

If we remove the restrictions of the Poincaré–Bendixson theorem, in such systems, chaos may occur through torus breakdown, period-doubling cascades, or resonance overlap. To substantiate this possibility, Figure 2 shows numerical evidence produced for representative parameter sets: (i) Time series, which are irregular, aperiodic oscillations in $\varphi(\xi)$ that do not settle into periodic or quasiperiodic patterns; (ii) a Poincaré section, which has scattered points instead of a closed invariant curve, indicating the destruction of a smooth torus; and (iii) the largest Lyapunov exponent, which is numerically estimated as positive ($\lambda_{max} > 0$), confirming sensitivity to initial conditions. These indicators support the conclusion that the periodically forced system may indeed enter a chaotic regime for sufficiently strong or resonant perturbations. We emphasize that the goal here is to demonstrate the possibility and qualitative nature of chaotic responses, rather than to undertake a full classification of chaotic attractors. A systematic analysis (including global bifurcation diagrams, continuation of the forcing amplitude, and rigorous Lyapunov spectral computations) is an interesting direction for future study, especially in relation to forced ion-acoustic oscillations.

According to the results above, the perturbed system (28) shows qualitatively different chaotic responses that are very sensitive to the exact shape of the external forcing. The phase portraits show

that changing the perturbation changes the flow's invariant geometry, which, in turn, changes the dynamic regimes that can be reached in the phase space. After describing how the system behaves qualitatively under different forcing scenarios, we will now focus on finding exact analytical solutions for the unperturbed model. Without outside forces acting on it (or with the right simplifying assumptions), the model supports several well-known types of traveling waves, such as solitary waves, spatially periodic (cnoidal) waves, and interactions between multiple solitons. A thorough derivation and examination of these solutions elucidate the model's inherent dynamics and clarify its fundamental integrability characteristics.

To clarify the role and motivation of the perturbation in Eq (28), we note that the term $R(\Omega) = 0.5\cos(2\Omega)$, $\Omega=\omega\tau+\varphi_0$, is chosen as the simplest smooth periodic forcing capable of modifying the invariant structure of the space–time fractional mKdV traveling wave system. Such sinusoidal forcing is commonly used in plasma models to represent weak oscillatory drivers (e.g., radio-frequency electric fields or low-frequency drift-wave modulations) and therefore provides a physically relevant means of probing the response of ion-acoustic structures to external excitation. Mathematically, this choice yields a periodically forced Duffing-type oscillator, which is a canonical system known to exhibit resonance, quasi-periodicity, and chaotic behavior under appropriate forcing amplitudes. In the present model, the perturbation breaks the Hamiltonian conservation of the unperturbed space–time fractional mKdV reduction and thereby permits dynamic regimes that do not arise in the two-dimensional autonomous system. To substantiate these effects, we provide numerical evidence in Figure 2, including aperiodic time series, scattered Poincaré sections, and a positive largest Lyapunov exponent for representative parameter values. These diagnostics demonstrate that the periodically forced fractional mKdV reduction can undergo torus breakdown and transition to chaos, consistent with the behavior of classical driven nonlinear oscillators. The perturbation analysis is therefore not intended to introduce a new dynamic framework, but rather to illustrate how external modulation qualitatively alters the wave dynamics relative to the unperturbed space-time fractional mKdV structure.

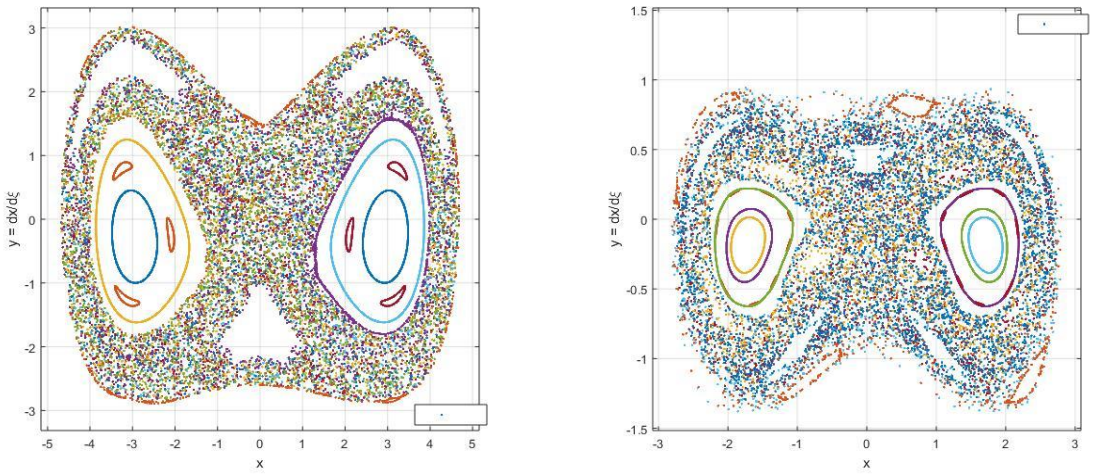

Figure 2. Phase portrait for the perturbed planar dynamic system in (26) under periodic forcing with $R(\Omega) = 0.5\cos(2\,\Omega)$ to two different values of the parameter: (a) $\omega = -1$, $k = -1$ and (b) $\omega = 1$, $k = 1$ with $\alpha = 1$, $A = 1$, and $B = 1$.

5. The fractional space–time mKdV equation's solitary wave solution

A solitary wave specifically refers to the transmission of a wave packet that is limited to a certain area. Moreover, solitons have nondispersive characteristics, indicating that they do not dissipate their energy during propagation. Moreover, their natural stability lets them move without losing energy, changing shape, or changing speed. The system's nonlinearity is what makes solitons possible. Solitons come from a steady balance between nonlinearity and dispersion, which makes a pulse that moves without changing form. To find a solitary solution, we rewrite Eq (26) as

$$\psi^2 = h + \frac{\alpha\omega}{k^3 B}\varphi^2 - \frac{A}{6k^2 B}\varphi^4. \tag{29}$$

Now, integrating along the level curves mentioned as $H(\varphi,\psi) = h$ gives

$$\psi = \int \frac{d\varphi}{\sqrt{h + \rho_1\varphi^2 - \rho_2\varphi^4}}, \qquad \rho_1 = \frac{\alpha\omega}{k^3 B}, \quad \rho_2 = -\frac{A}{6k^2 B}. \tag{30}$$

as Eq (30) interprets the parametric form of the analytical solutions, which corresponds to the level curves described by $H(\varphi,\psi) = h$, if $h = 0$, Eq (30) becomes

$$\psi = \int \frac{d\varphi}{\varphi\sqrt{\rho_1 - \rho_2\varphi^2}}. \tag{31}$$

This has the standard form whose localized solution is

$$\varphi(\zeta) = \pm\sqrt{\frac{\rho_1}{\rho_2}}\,\mathrm{sech}(\sqrt{\rho_1}\,(\zeta - \zeta_0)). \tag{32}$$

With an arbitrary shift ζ_0. Substituting ρ_1 and ρ_2 yields

$$\varphi(\zeta) = \pm\sqrt{\frac{6\alpha\omega}{Ak}}\,\mathrm{sech}\left(\sqrt{\frac{\alpha\omega}{k^3 B}}\,\frac{(k\xi^\alpha - \alpha\omega\tau^\alpha - \zeta_0)}{\alpha}\right), \tag{33}$$

where $A_m = \sqrt{\frac{6\alpha\omega}{Ak}}$ and $W = \sqrt{\frac{\alpha\omega}{k^3 B}}$ represent the amplitude and width of the soliton.

Before examining the detailed influence of the fractional order on soliton propagation, it is instructive to first assess its effect on key wave characteristics (namely the phase velocity V, amplitude A_m, width W, and the overall soliton structure governed by the space–time fractional mKdV equation). In this analysis, particular attention is given to three fundamental plasma parameters: (i) The temperature ratio $\delta = T_h/T_c$ between hot and cool electrons, and (ii) the nonextensivity indices q_c and q_h, which quantify deviations of the cool and hot electron populations

from Maxwellian equilibrium. In Figure 3(a), we can see that the phase velocity starts out somewhat high and then goes down as the temperature ratio δ goes up. But when fractional effects are considered, the velocity graph always goes up as the fractional order goes down. This shows that the speed of transmission goes up no matter what physical factors are at play. Figure 3(b) also demonstrates that, in the classical limit, the phase velocity remains essentially constant with increasing q_c; however, in the fractional regime, the velocity increases monotonically as α decreases. Finally, Figure 3(c) reveals that the phase velocity decreases with increasing q_h in the integer-order model, whereas decreasing the fractional order again produces an upward displacement of the curve. Collectively, these results show that the fractional order α can be used as a separate and very effective control parameter to raise the phase velocity without changing the plasma's basic properties. This gives us a new way to fine-tune how waves travel through complex plasma environments.

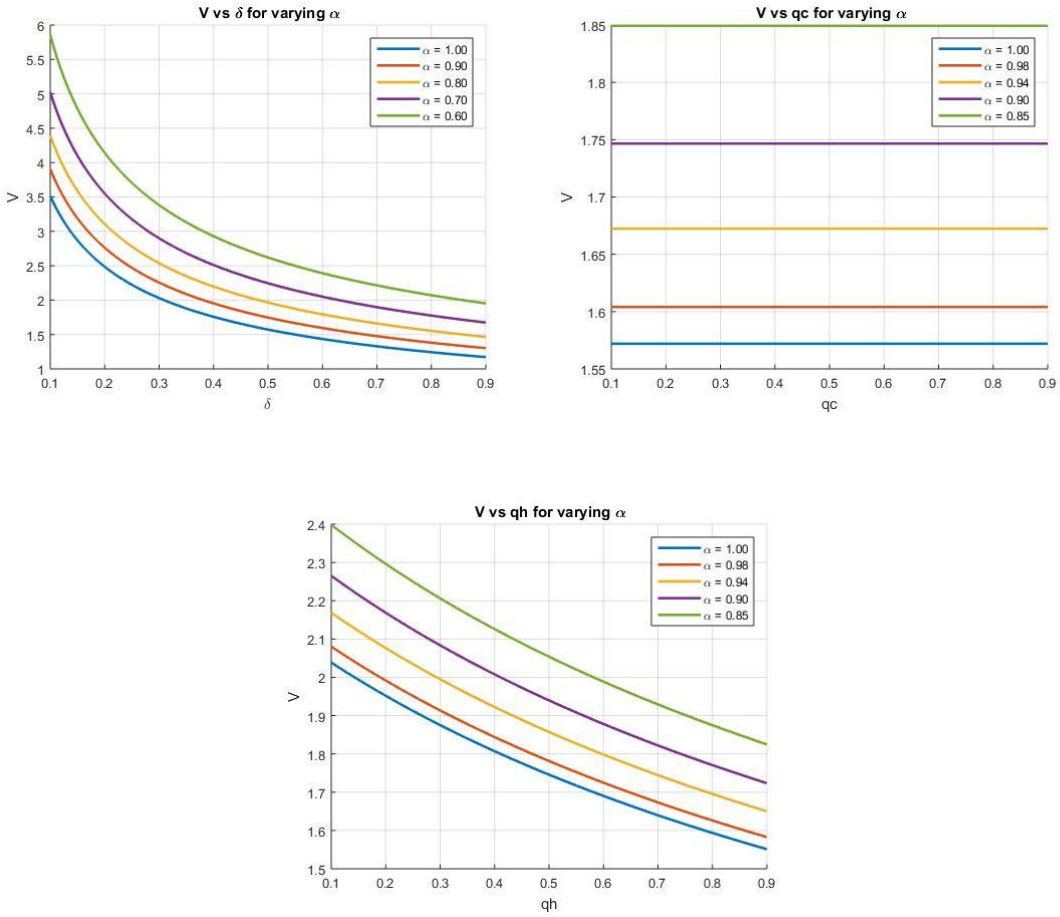

Figure 3. The impact of V vs. $\{\delta, q_c, q_h\}$ with varying α.

Figure 4 illustrates the dependence of the soliton's amplitude A_m on the temperature ratio δ, the nonextensivity indices q_c and q_h, and the fractional order α. As shown in Figure 4(a), the amplitude initially assumes a relatively large value and then decreases as δ increases. When fractional effects are incorporated, the amplitude curves consistently shift downward as the fractional order decreases, indicating that α exerts a dominant influence on the reduction in amplitude regardless of the underlying plasma parameters. Figure 4(b) also indicates that, in the classical limit, the amplitude remains nearly

constant with an increasing q_c; however, in the fractional regime, A_m decreases monotonically as α decreases. A similar trend is evident in Figure 4(c), where the amplitude decreases with an increasing q_h in the integer-order case, whereas lowering α produces an even more pronounced downward shift. Taken together, these results demonstrate that the fractional order α serves as an independent and highly sensitive control parameter capable of modifying the solitons' amplitude without the need to adjust the intrinsic plasma characteristics. This provides an additional degree of flexibility for tuning waves' behavior in complex plasma environments.

Figure 5 presents the variation in the soliton width W with respect to the temperature ratio δ, the nonextensivity parameters q_c and q_h, and the fractional order α. As shown in Figure 5(a), the soliton's width begins with a relatively small value and increases as δ increases. When fractional effects are introduced, the corresponding width curves exhibit a systematic downward shift as the fractional order decreases, demonstrating that α plays a primary role in reducing the spatial extent of the soliton irrespective of the plasma parameters. Figure 5(b) shows that, in the classical limit, the width remains nearly unchanged with an increasing q_c; however, in the fractional regime, the width decreases monotonically with a decreasing α. A comparable behavior is observed in Figure 5(c), where the width increases with an increasing q_h in the integer-order model, while lower fractional orders again lead to a notable downward displacement of the width profile. These observations confirm that the fractional order α acts as a distinct and highly sensitive control parameter capable of tailoring the soliton's width without modifying the intrinsic plasma characteristics. Therefore, the fractional framework adds another level of control for managing how nonlinear waves move in complicated plasma settings.

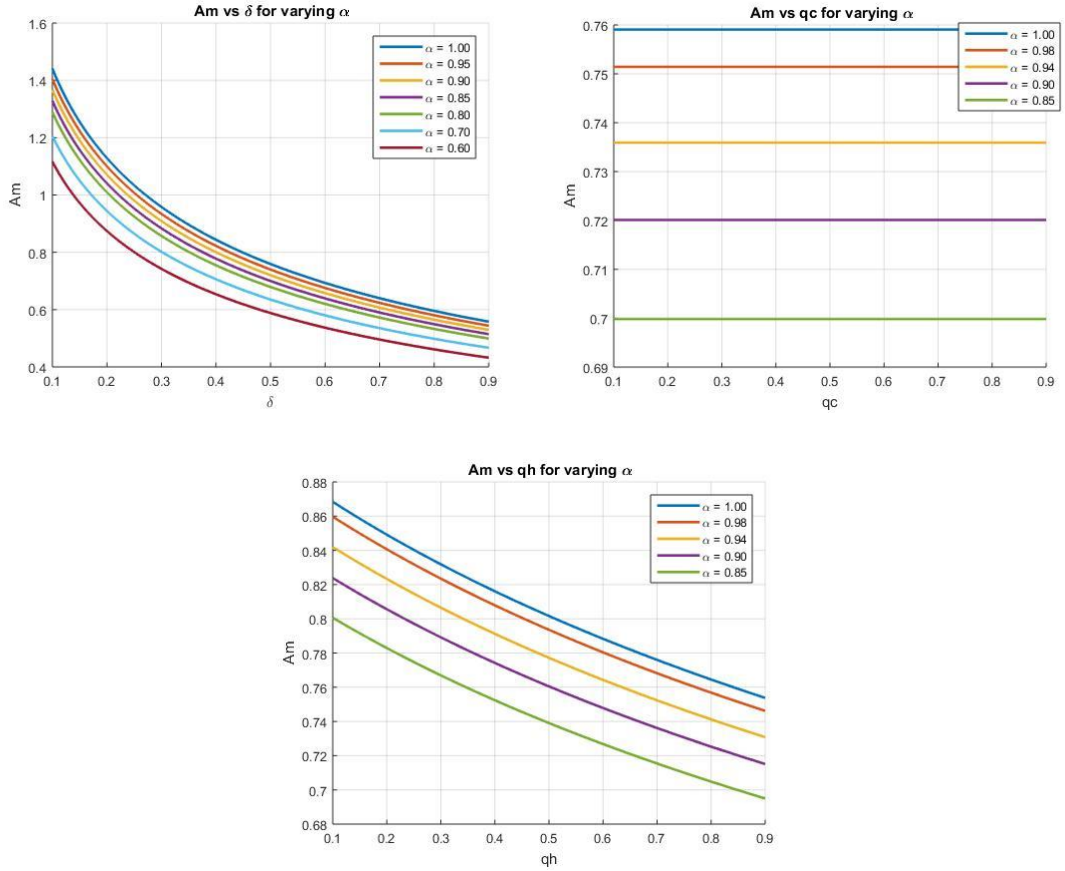

Figure 4. The impact of A_m vs. $\{\delta, q_c, q_h\}$ with varying α.

Figure 6 illustrates the propagation of the soliton solution φ of the space–time fractional KdV equation (cf. Eq (33)) for several values of the fractional order α that represents a bright soliton solution. Figure 6(a) presents a three-dimensional surface for the classical case α=1. Figure 6(b) shows the two-dimensional cross-section at $\tau = 20$ for different values of α = 1, 0.98, 0.96, 0.94, 0.92, and 0.8. Figure 6(c) gives a three-dimensional view for $\alpha = 0.9$, the corresponding two-dimensional cross-sections at $\tau = 20$ are shown in Figure 6(d) for different values of α = 0.9, 0.88, 0.86, 0.84, 0.82, and 0.8. Figure 6(e) provides a three-dimensional view for $\alpha =$ 0.8, and the two-dimensional cross-sections at $\tau = 20$ are shown in in Figure 6(f) for different values of α = 0.8, 0.78, 0.76, 0.74, 0.72, and 0.7 when $\vartheta = 0.5, q_c = 0.5, q_h = 0.86,$ $k_1 = 0.2, \delta = 0.3, k_2 = 0.4, \omega = 0.5,\ k = 10, \zeta_0 = 370$ and $B_0 = 0.5$.

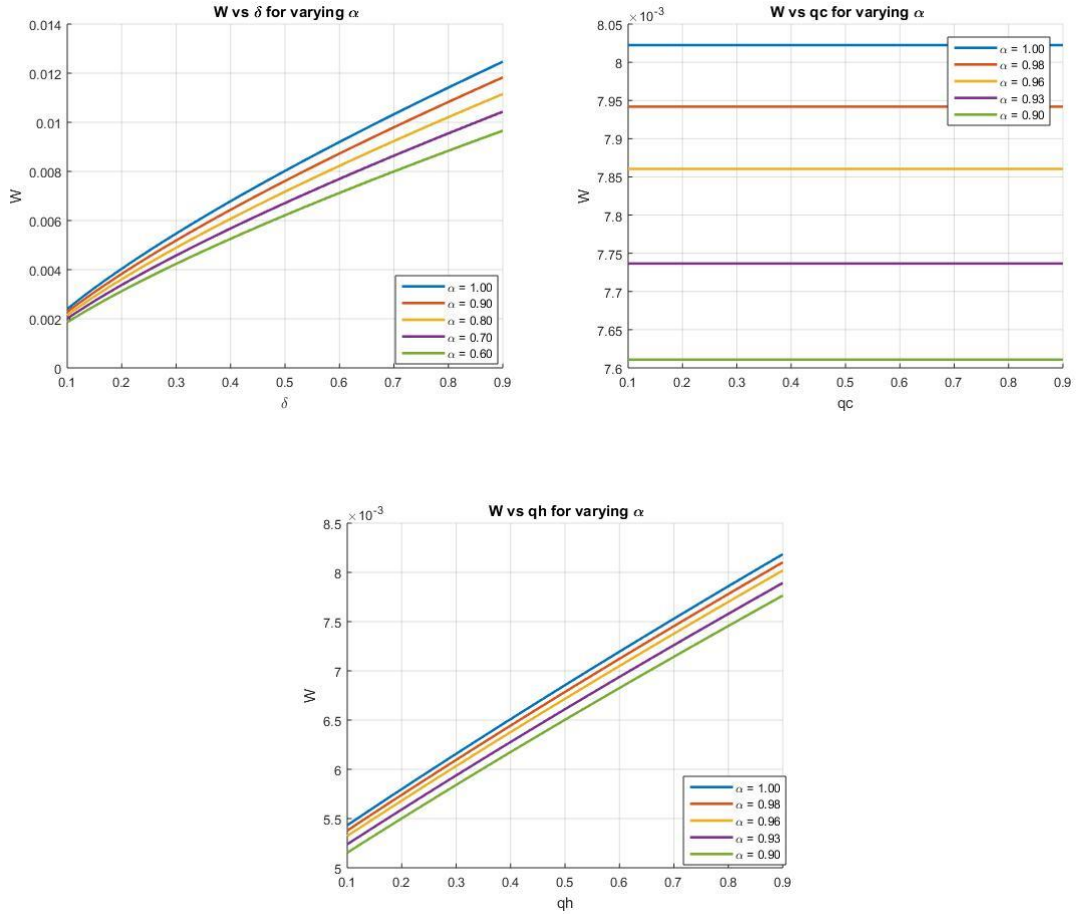

Figure 5. The impact of W vs. $\{\delta, q_c, q_h\}$ with a varying α.

Across all subfigures, a clear and systematic dependence on the fractional order is observed: As α decreases, the soliton's peak amplitude diminishes while its spatial width increases. This indicates that lowering α effectively enhances the dispersive contribution relative to the nonlinear steepening mechanism, thereby producing broader and weaker ion-acoustic solitary waves. Such behavior quantitatively highlights the role of the fractional order in shaping the waveform's morphology and propagation properties. For completeness, we note that selecting the negative sign in Eq (33) yields the corresponding dark soliton family, which exhibits an analogous monotonic sensitivity to α, as shown in Figure 7.

It is evident that when α=1, the solution in Eq (33) reduces exactly to the classical bright soliton solution of the standard mKdV equation. This limiting behavior confirms that the fractional model is fully consistent with established integer-order theory. The results obtained here therefore validate both the reliability and accuracy of the derived solutions across the parameter ranges considered. Moreover, the smooth recovery of the classical mKdV waveform demonstrates that the fractional solutions correctly reproduce known physical behavior whenever the governing dynamics revert to their classical regime. Since the nonlinear wave evolution in both the integer-order and fractional settings is governed by the same underlying balance between dispersion and nonlinearity, these findings reinforce the capability of the present model to capture ion-acoustic wave dynamics with high fidelity.

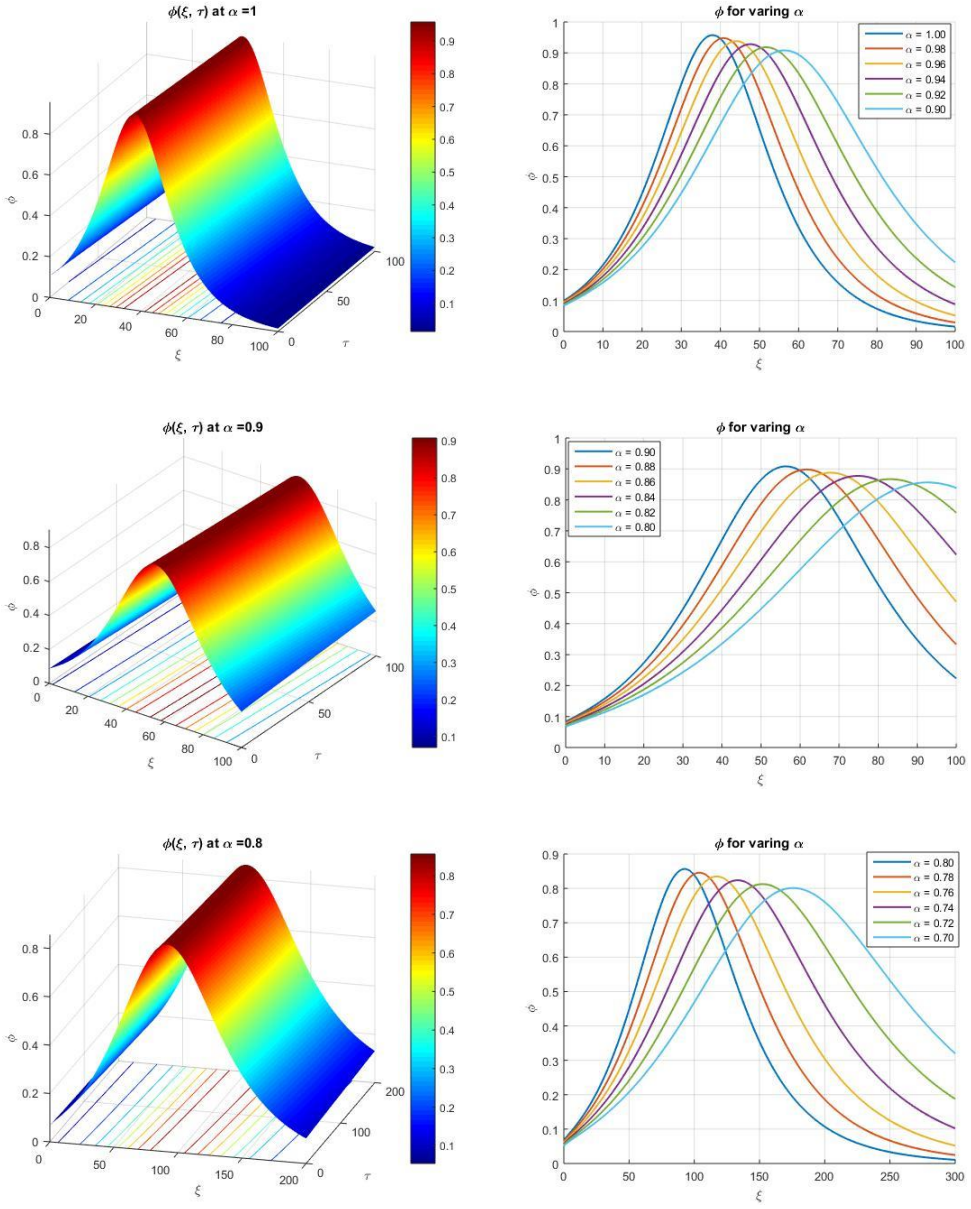

Figure 6. The propagation of the soliton solution ϕ of the space–time fractional KdV equation for different values of α when $\vartheta = 0.5, q_c = 0.5, q_h = 0.86,\ k_1 = 0.2,\ \delta = 0.3,\ k_2 = 0.4, \omega = 0.5,\ k = 10, \zeta_0 = 370$, and $B_0 = 0.5$.

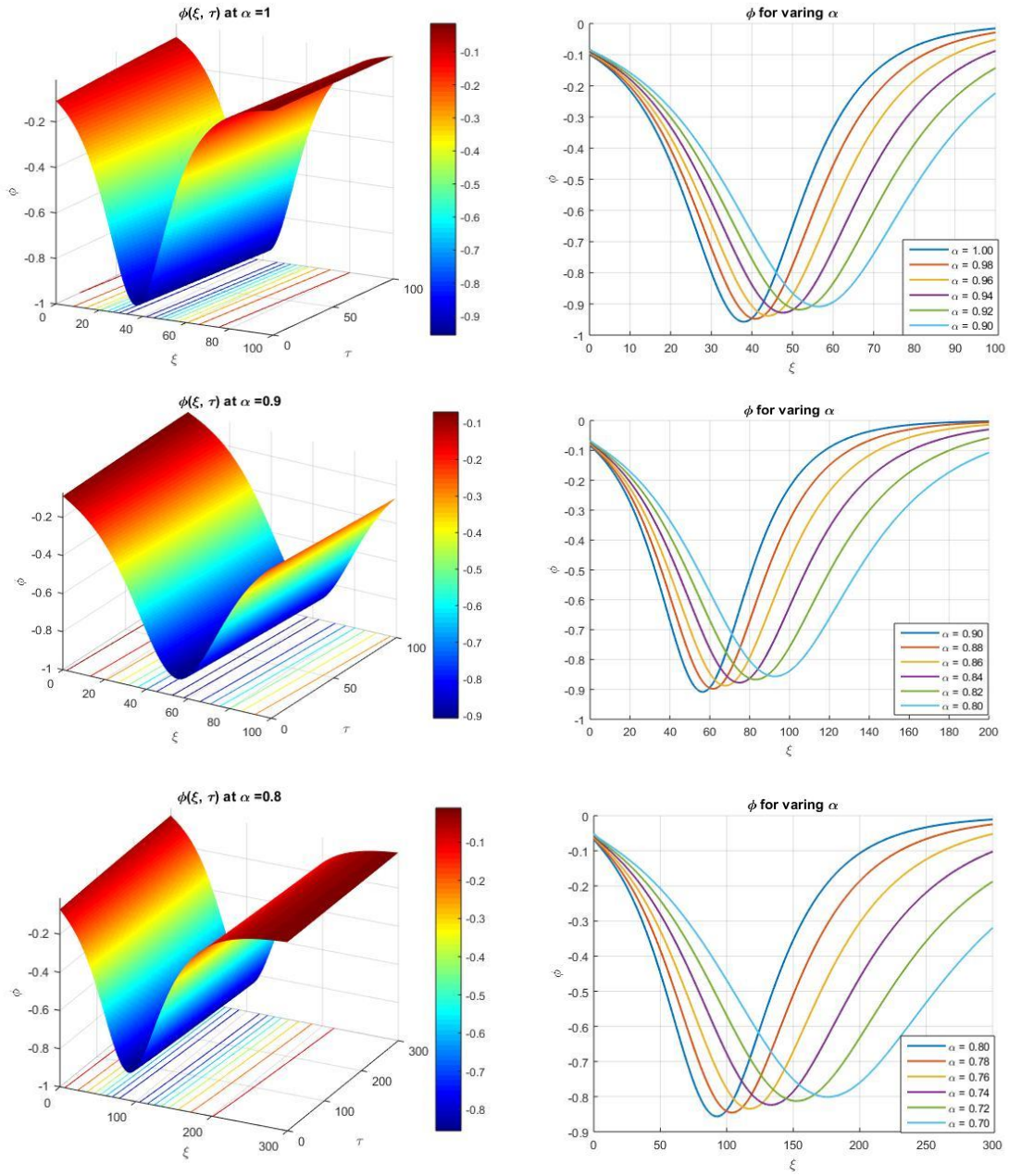

Figure 7. The propagation of the soliton solution ϕ of Eq (33) with a negative sign for different values of α when $\vartheta = 0.5, q_c = 0.5, q_h = 0.86,\ k_1 = 0.2,\ \delta = 0.3,$ $k_2 = 0.4, \omega = 0.5,\ k = 10, \zeta_0 = 370$, and $B_0 = 0.5$.

5.1. Tanh-function solution (kink wave solution)

The kink wave solution is a monotone traveling wave that connects two distinct constant states as $\xi \to \pm\infty$. For our mKdV traveling ODE, it is a heteroclinic orbit satisfying

$$\lim_{\zeta \to \pm\infty} \varphi(\zeta) = \pm\rho, \qquad \rho = \sqrt{3\alpha\omega / A\,k},$$

with $\zeta = (k\,\xi^{\alpha} - \alpha\omega\tau^{\alpha})/\alpha$. By utilizing the traveling wave transformation (21) in the space–time

fractional mKdV Eq (18), we derive the ordinary differential Eq (23). Integrating (23) with respect to ζ and setting the integration constant to zero yields

$$\varphi'' = \frac{\alpha\omega}{k^3 B}\varphi - \frac{A}{3k^2 B}\varphi^3. \tag{34}$$

Multiplying Eq (34) by φ' and integrating with respect to ζ, we have

$$\varphi'' = \frac{\alpha\omega}{k^3 B}\varphi^2 - \frac{A}{6k^2 B}\varphi^4 + \frac{2C}{k^3 B}, \tag{35}$$

where C is an integration constant. Taking $C = -3\alpha^2\omega^2/(4Ak)$, we have

$$\begin{aligned} \varphi'^2 &= -\frac{A}{6k^2 B}\left(\varphi^4 - \frac{6\alpha\omega}{kA}\varphi^2 + \frac{9\alpha^2\omega^2}{A^2k^2}\right) \\ &= -\frac{A}{6k^2 B}\left(\frac{3\alpha\omega}{kA} - \varphi^2\right)^2. \end{aligned} \tag{36}$$

By separating variables and integration, we have

$$\varphi(\zeta) = \pm\sqrt{\frac{3\alpha\omega}{Ak}}\tanh\left(\sqrt{\frac{\alpha\omega}{2k^3 B}}(\zeta - \zeta_0)\right), \tag{37}$$

where $\sqrt{\frac{3\alpha\omega}{Ak}}$ and $\sqrt{\frac{\alpha\omega}{2k^3 B}}$ represent the amplitude and width of the kink soliton. Kinks are canonical solitonic transition layers, which are monotone traveling waves that connect different asymptotic states and stay the same even when they are disturbed weakly. They appear in fluid dynamics, plasma physics, nonlinear optics, magnetism, and condensed matter systems as strong interfaces or domain walls. Kinks are not only useful for theory; they also support technologies that use controllable changes between states, like materials for storing information and converting energy. Characterizing their amplitude–speed relation, width, and stability gives designers a way to make devices that route, store, or change energy and information. Ongoing work continues to connect advanced mathematical theory (existence, stability, interactions) with practical uses, which helps us better predict, control, and create sharp changes in complex media. When the fractional order approaches one, the solution in (37) also becomes the standard kink solution of the mKdV equation. This change shows that the standard model's usual behaviors are having an increasingly larger impact on how the system works. The use of this well-known approach will make it possible for users to choose the most effective treatment and understand how it operates. A comparison of the data from the traditional framework with the data from the new formulation demonstrates that the derived family is accurate. Within the framework of the mKdV equation and its fractional extensions, the model is able to provide an accurate explanation and forecast the occurrence of nonlinear wave phenomena. The ability to deal with real-world applications in fields such as fluid dynamics and plasma physics has been enhanced as a direct consequence of these findings. Our ability to perform a more in-depth analysis of complex systems and the behaviors that they exhibit has been made

feasible as a result. Therefore, scientists may utilize this as a spark to explore events that have not been documented before and to build upon ideas that have already been established. Figure 8 depicts the propagation of the kink soliton solution φ of the space–time fractional KdV equation (cf. Eq (37)) for several values of the fractional order α. In order to analyze and grasp the properties of the kink solution in a more straightforward manner, it is possible to make use of this well-known framework. In light of the findings of this consistency check, which substantiates the correctness of the derived family, it has been established that the proposed formulation produces the same results as the traditional framework. Consequently, this demonstrates that the formulation that was suggested is exactly correct. The model makes it possible to precisely describe and anticipate the appearance of nonlinear wave phenomena that are controlled by the mKdV equation and its fractional extensions. The use of the approach makes this a realizable possibility. We are now in a position to dive more thoroughly into the dynamics of complex systems and to improve our capacity to solve practical difficulties in domains such as plasma physics and fluid dynamics. This is all thanks to the new understandings that we have gained. The fact that we now have a deeper comprehension of these subjects is the primary reason for this positive development. In light of this, scientists have the opportunity to make use of this to their advantage by investigating hitherto unknown occurrences and strengthening already established concepts.

Figure 5 depicts the propagation of the kink soliton solution φ of the space–time fractional KdV equation (cf. Eq (37)) for several values of the fractional order α. Figure 8(a) presents a three-dimensional surface for the classical case α=1; Figure 8(b) shows the two-dimensional cross-sections at a fixed time $\tau = 20$ for α∈ {1, 0.98, 0.96, 0.94, 0.92, 0.80}. Figure 8(c) provides a three-dimensional view for α=0.9, with the corresponding cross-sections at $\tau = 20$ reported in Figure 8(d) for α∈ {0.90, 0.88, 0.86, 0.84, 0.82, 0.80}. Figure 8(e) gives a three-dimensional view for α = 0.8, and Figure 8(f) displays cross-sections at $\tau = 20$ for α∈ {0.80, 0.78, 0.76, 0.74, 0.72, 0.70} when $\vartheta = 0.5, q_c = 0.5, q_h = 0.86, \ k_1 = 0.2, \ \delta = 0.3, \ k_2 = 0.4, \omega = 0.5, \ k = 10, \zeta_0 = 370$, and $B_0 = 0.5$.

Across all subfigures, a clear dependence on the fractional order is observed: As α decreases, the kink's profile becomes progressively smoother, exhibiting reduced front steepness and an increasingly broadened transition layer. This behavior indicates that lowering α enhances the effective dispersive contribution relative to the nonlinearity, leading to more gradual ion-acoustic transitions. These trends quantify the influence of the fractional order on the waveform's morphology and propagation dynamics. Finally, selecting the opposite sign in Eq (37) generates the corresponding antikink solutions, which display the same qualitative dependence on α as shown in Figure 9.

When α=1, the solution given in Eq (37) recovers the classical kink soliton of the standard mKdV equation. This limiting case provides a direct analytical check of consistency, demonstrating that the fractional formulation smoothly reduces to the well-established integer-order model. The agreement with the classical solution confirms the correctness of the derived waveforms and ensures that the fractional extensions do not introduce spurious behavior. Moreover, the preservation of the underlying nonlinear–dispersive balance in both the fractional and classical regimes reinforces the ability of the present model to represent ion-acoustic wave dynamics accurately across a broad range of parameter values.

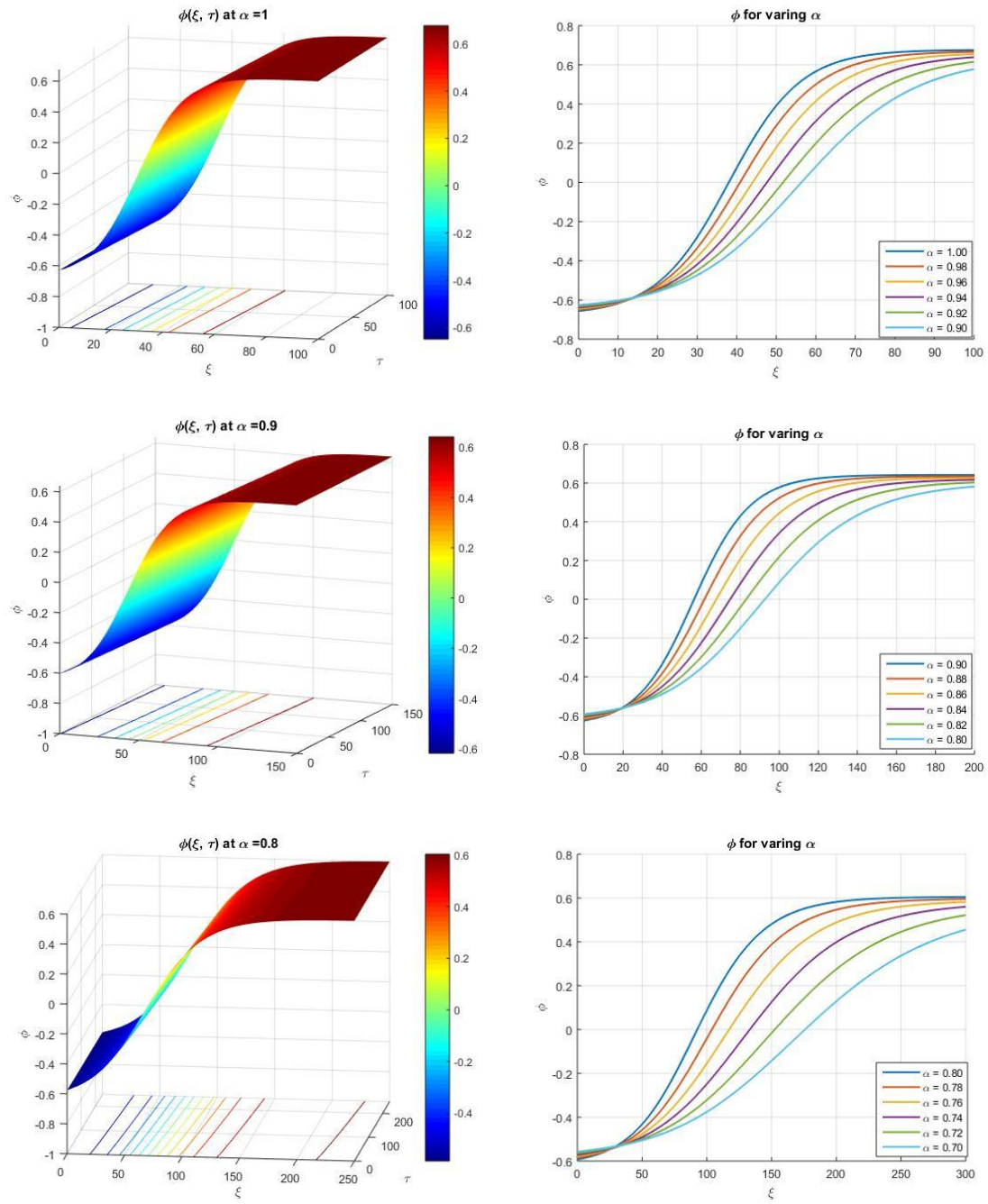

Figure 8. The propagation of the kink soliton solution ϕ given by Eq (37) for different values of α when $\vartheta = 0.5, q_c = 0.5, q_h = 0.86,$ $k_1 = 0.2,$ $\delta = 0.3,$ $k_2 = 0.4, \omega = 0.5,$ $k = 10, \zeta_0 = 370$, and $B_0 = 0.5$.

5.2. Jacobi elliptic function solution (double periodic wave solution)

Doubly periodic traveling waves have regular oscillations that happen at specified times and places and then recur. This leads to the creation of intricate structures that resemble lattices. In fluid dynamics and nonlinear optical systems, where the combination of dispersion and nonlinearity results in sophisticated dynamic interactions, it is particularly beneficial for modeling

finite-amplitude wave trains. This is because it allows for the modeling of wave trains with smaller amplitudes. The framework in question is very useful for accomplishing this objective. These technologies let users work with waveform properties with high accuracy. These characteristics include aspects like modulation, amplitude, wavelength, and mean level. As a consequence, these methods affect many different areas, such as constructed metamaterials, photonic lattices, and telecommunications that regulate dispersion, to name a few. Researchers may make and change waveforms for practical uses by leveraging their customizable qualities. This helps to advance technology in the fields of signal transmission, information processing, and materials science. This lets them create and change waveforms.

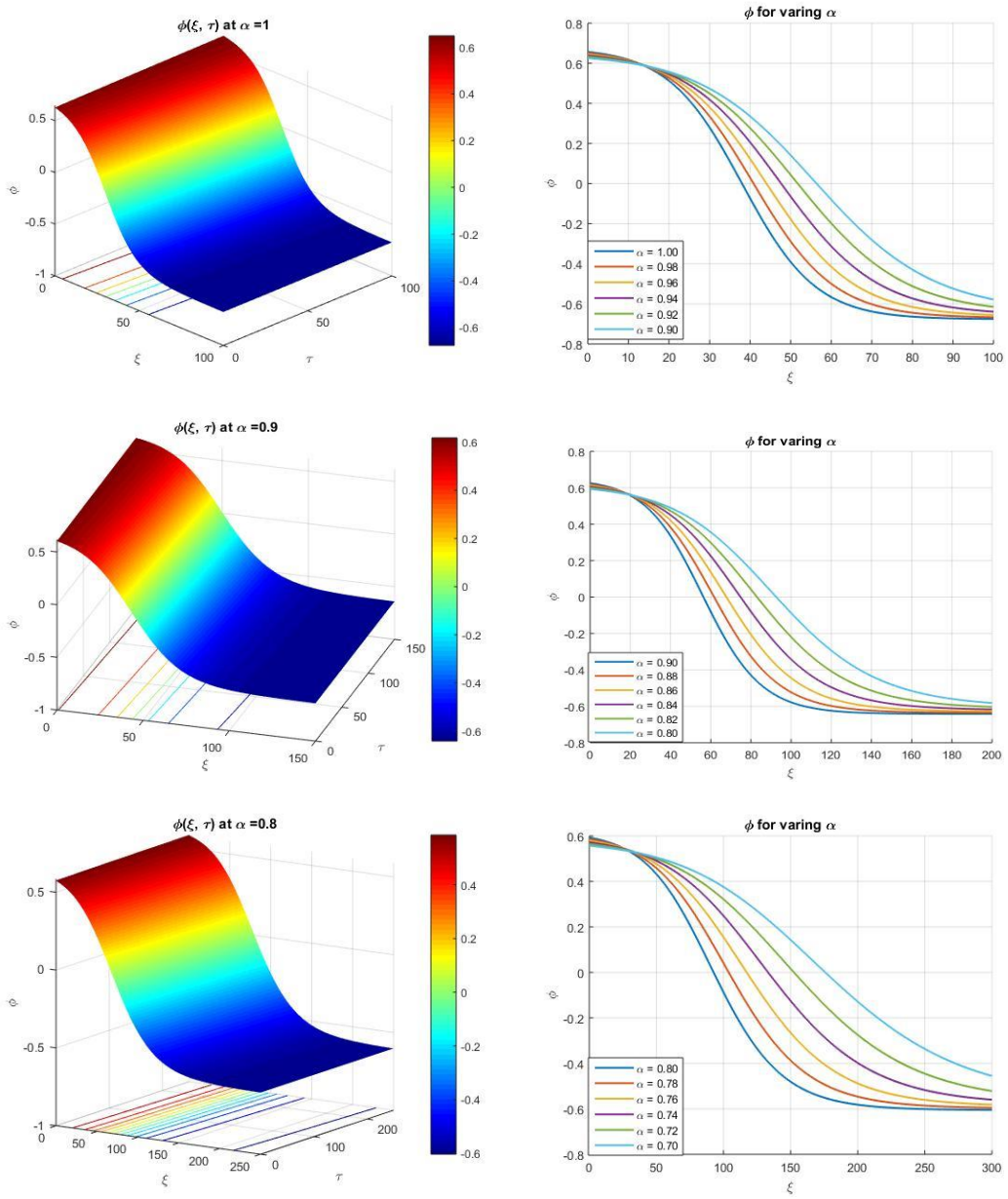

Figure 9. The propagation of the antikink soliton solution ϕ given by the negative sign of Eq (37) for different values of α when $\vartheta = 0.5, q_c = 0.5, q_h = 0.86,\ k_1 = 0.2,$ $\delta = 0.3,\ k_2 = 0.4, \omega = 0.5,\ k = 10, \zeta_0 = 370$, and $B_0 = 0.5$.

In this context, Jacobi elliptic solutions (represented by sn, cn, and dn) provide a precise and

computationally efficient characterization of real-line periodic wave trains for mKdV-type models, while their complex analytic double periodicity integrates them seamlessly into finite-gap theory (one solution). Altering the elliptic modulus $m\in(0,1)$ creates a seamless transition from small-amplitude, virtually sinusoidal waves ($m\to 0^{+}$) to the solitary-wave limits ($m\to 1^{-}$), where cn and dn approach sech (bright pulses) and sn approaches tanh (kinks/antikinks). These restrictive connections guarantee alignment with classical solitary wave phenomenology and provide a cohesive analysis across linear, weakly nonlinear, and highly nonlinear domains, thus aiding in stability investigations, asymptotic simplifications, and quantitative comparisons with experimental data.

The following are the Jacobi elliptic traveling wave solutions for the mKdV equation:

$$-\alpha\,\omega\varphi'+kA\,\varphi^{2}\,\varphi'+k^{3}B\,\varphi'''=0,\quad \zeta=k\,\xi-\omega\tau,\ '=d\,/\,d\,\zeta. \tag{38}$$

Integrating (38) with respect to ζ and setting the integration constant to zero yields

$$-\alpha\,\omega\varphi+\frac{kA}{3}\varphi^{3}+k^{3}B\,\varphi''=0,$$

which can be written equivalently as

$$\varphi''=\rho_1\varphi-\rho_2\varphi^{3}, \tag{39}$$

where $\rho_1=\dfrac{\alpha\,\omega}{k^{3}B}$, $\rho_2=\dfrac{A}{3k^{2}B}$. Utilizing these identities about their argument z, we have

$$\begin{aligned}
&\frac{d^{2}}{dz^{2}}\mathrm{sn}(z,m)=-(1+m)\,\mathrm{sn}(z,m)+2m\,\mathrm{sn}^{3}(z,m),\\
&\frac{d^{2}}{dz^{2}}\mathrm{cn}(z,m)=(2m-11)c\mathrm{n}(z,m)-2m\ \mathrm{cn}^{3}(z,m),\\
&\frac{d^{2}}{dz^{2}}\mathrm{dn}(z,m)=(2-m)\,\mathrm{dn}(z,m)-2\,\mathrm{dn}^{3}(z,m).
\end{aligned} \tag{40}$$

I) A snoidal wave has the form (sn function)

$$\varphi(\zeta)=\pm\sqrt{\frac{6m\,\alpha\omega}{Ak\,(1+m)}}\,\mathrm{sn}\left(\sqrt{\frac{\alpha\omega}{k^{3}B\,(1+m)}}\,(\zeta-\zeta_0),m\right). \tag{41}$$

II) A cnoidal wave has the form (cn function)

$$\varphi(\zeta)=\pm\sqrt{\frac{6m\,\alpha\omega}{Ak\,(2m-1)}}\,\mathrm{cn}\left(\sqrt{\frac{\alpha\omega}{k^{3}B\,(2m-1)}}\,(\zeta-\zeta_0),m\right). \tag{42}$$

III) A dnoidal wave has the form (dn function)

$$\varphi(\zeta)=\pm\sqrt{\frac{6m\,\alpha\omega}{Ak\,(2-m)}}\,\mathrm{dn}\left(\sqrt{\frac{\alpha\omega}{k^{3}B\,(2-m)}}\,(\zeta-\zeta_0),m\right). \tag{43}$$

When $m \to 1$, we have $\mathrm{sn}(z,1) = \tanh(z)$, which gives

$$\varphi(\zeta) = \pm\sqrt{\frac{3\alpha\omega}{Ak}}\tanh\left(\sqrt{\frac{\alpha\omega}{2k^3B}}(\zeta - \zeta_0)\right). \tag{44}$$

This is the same as Eq (37). In addition, when $m \to 1$, we get $\mathrm{cn}(z,1) = \mathrm{dn}(z,1) = \mathrm{sech}(z)$, which gives

$$\varphi(\zeta) = \pm\sqrt{\frac{6\alpha\omega}{Ak}}\,\mathrm{sech}\left(\sqrt{\frac{\alpha\omega}{k^3B}}(\zeta - \zeta_0)\right). \tag{45}$$

This is the same as Eq (33).

5.3. Technique of the Kudryashov expansion

To independently verify the traveling wave solutions obtained in the previous subsections, we apply the Kudryashov expansion method, a widely used symbolic technique for nonlinear evolution equations. The method is based on balancing the highest-order derivative term with the strongest nonlinear term in the reduced ODE. For Eq (34), balancing φ'', and φ^3, yields $N+2 = 3N$, and the answer is found to be $N = 1$, which implies that the solution can be expressed as a first-order truncated expansion in the auxiliary function.

$$\varphi(\zeta) = a_0 + a_1\psi(\zeta). \tag{46}$$

When $\psi(\zeta) = \dfrac{1}{1+\rho\, e^{\mu\zeta}}$ satisfies $\psi' = \mu\psi(\psi - 1)$, obtaining the first and second derivatives of the function φ is necessary in order to substitute Eq (46), which is a part of Eq (34)

$$\begin{aligned} \varphi' &= a_1\mu(\psi^2 - \psi), \\ \varphi'' &= a_1\mu(2\psi - 1)\psi' \\ &= a_1\mu^2(2\psi^3 - 3\psi^2 + \psi). \end{aligned} \tag{47}$$

When we put Eqs (46) and (47) into (34), we get

$$-\alpha\,\omega(a_0 + a_1\psi) + \frac{kA}{3}(a_0 + a_1\psi)^3 + a_1\mu^2k^3B\,(2\psi^3 - 3\psi^2 + \psi) = 0.$$

If we collect the coefficients of similar powers of ψ, we get the following system of nonlinear algebraic equations:

$$\begin{aligned} \psi^0 &: \quad a_0(3\alpha\,\omega - kAa_0^2) = 0, \\ \psi &: \quad a_1(-\alpha\,\omega + kAa_0^2 + \mu^2k^3B) = 0, \\ \psi^2 &: \quad a_1(kAa_1a_0 - 3\mu^2k^3B) = 0, \\ \psi^3 &: \quad a_1(kAa_1^2 + 6\mu^2k^3B) = 0. \end{aligned}$$

Through the process of solving the resulting system of four equations, the following outcomes are obtained:

$$a_1 = -2a_0, \quad a_0 = \pm\sqrt{\frac{\alpha\omega}{3kA}}, \quad \mu = \sqrt{\frac{2\alpha\omega}{k^3 B}}. \tag{48}$$

A comprehensive understanding of the nonlinear behavior that lurks under the surface may be obtained via the use of this analytical approach. In addition, in order to carry out the task of describing the wave, it is possible to get a precise description of the wave's profile. This particular formulation is a perfect illustration of how robust the Kudryashov technique is when it comes to the resolution of issues that include nonlinear development. It is noteworthy that this formulation demonstrates the ability to consistently discover solutions for solitary waves that have apparent physical importance. This formulation is a particular example of this capability. As a consequence of this, the precise reaction may be characterized as follows:

$$\varphi(\zeta) = \pm\sqrt{\frac{\alpha\omega}{3kA}}\left[1 - \frac{2}{1+\rho\, e^{\sqrt{\frac{2\alpha\omega}{k^3 B}}\,\zeta}}\right]. \tag{49}$$

The Kudryashov index, proposed in Eq (49), is a designated parameter. This parameter delineates the kind of wave solutions generated. This method has a significant function. Singular wave profiles correspond to a value of ρ that is less than zero. The wave profiles are marked by sudden gradients or infinite amplitudes in certain instances. These wave profiles may reflect several physical processes, including energy localization and the waves breaking. If ρ exceeds 0, normal (nonsingular) kink-type waves are generated. These waves display a transition that is both smooth and monotonic between two asymptotic states, and they continue to keep their amplitude constant during their entire lifespan. Consequently, Eq (34) may characterize both traditional kink-type waves, which are often seen in stable propagation environments, and their singular counterparts, which are generally associated with unstable or highly localized energy concentrations in nonlinear media.

If we take $\rho = e^{\sqrt{\frac{2\alpha\omega}{k^3 B}}\,\zeta_0}$, we have $1 - \frac{2}{1+e^{\sqrt{\frac{2\alpha\omega}{k^3 B}}\,(\zeta-\zeta_0)}} = \tanh\left(\frac{1}{2}\sqrt{\frac{2\alpha\omega}{k^3 B}}\,(\zeta-\zeta_0)\right)$, and then Eq (49) take the form

$$\varphi(\zeta) = \pm\sqrt{\frac{3\alpha\omega}{Ak}}\tanh\left(\sqrt{\frac{\alpha\omega}{2k^3 B}}\,(\zeta-\zeta_0)\right).$$

This is the same as Eq (37).

Note that the Kudryashov expansion does not produce new solution families beyond those obtained earlier through the elliptic function method or direct quadrature. Instead, it provides an independent algebraic construction of the same traveling wave profiles, confirming the correctness and consistency of the earlier solutions.

5.4. Analytical solitary solution of the space–time fractional mKdV equation

We use the F-expansion method to get precise analytic solutions for the space–time fractional mKdV model. The F-expansion method is an effective and direct algebraic strategy for obtaining exact solutions to nonlinear evolution problems [47], and it has been used to resolve various nonlinear equations. We examine the fractional space–time mKdV equation in its present form, as delineated in Eq (18). We implement the traveling wave transformation defined as $\varphi(\xi^{\alpha},\tau^{\alpha})=\varphi(\zeta)$ and $\zeta=(k\,\xi^{\alpha}-\alpha\omega\tau^{\alpha})/\alpha$. Consequently, Eq (18) is transformed into the following ODE:

$$-\alpha\,\omega\frac{d\varphi}{d\zeta}+kA\,\varphi^{2}\frac{d\varphi}{d\zeta}+k^{3}B\,\frac{d^{3}\varphi}{d\zeta^{3}}=0, \tag{50}$$

The space–time fractional mKdV model can be solved by using the F-expansion method as follows:

$$\varphi(\zeta)=a_0+\sum_{j=1}^{N}a_j F^{j}(\zeta),\qquad a_N\neq 0,\quad F'=\sqrt{\rho_0+\rho_1F^{2}+\rho_2F^{4}}, \tag{51}$$

where $a_0,a_1,...,a_N$ are arbitrary constants. *N= 1* can be obtained by balancing the highest-order linear partial derivative term and the highest-order nonlinear term in Eq (50). Equation (50) has the following solution:

$$\varphi(\zeta)=a_0+a_1F(\zeta). \tag{52a}$$

From Eq (52a), we have

$$\begin{aligned}
&\frac{d\varphi}{d\zeta}=a_1\sqrt{\rho_0+\rho_1F^{2}+\rho_2F^{4}},\\
&\varphi\frac{d\varphi}{d\zeta}=a_1\left(a_0+2a_0a_1F+a_1^{2}F^{2}\right)\sqrt{\rho_0+\rho_1F^{2}+\rho_2F^{4}},\\
&\frac{d^{3}\varphi}{d\zeta^{3}}=a_1\left(\rho_1+6\rho_2F^{2}\right)\sqrt{\rho_0+\rho_1F^{2}+\rho_2F^{4}}.
\end{aligned} \tag{52b}$$

Substituting Eqs (52a) and (52b) in (50), we have

$$a_1\left(-\alpha\,\omega+kA\left(a_0+2a_0a_1F+a_1^{2}F^{2}\right)+k^{3}B\left(\rho_1+6\rho_2F^{2}\right)\right)\sqrt{\rho_0+\rho_1F^{2}+\rho_2F^{4}}=0.$$

Collecting the coefficients of $F(\zeta),\ i=0,1,...$ and setting the coefficients equal to zero, and solving this system, we obtain the following solution for the parameters ω,a_0,a_1, and k:

$$a_0=0,\qquad a_1=\pm\sqrt{-\frac{6k^{2}B\,\rho_2}{A}},\qquad \alpha\,\omega=k^{3}B\,\rho_1. \tag{53}$$

The electrostatic potential can be determined using the IASW solution by substituting from Eq (54) into (51). We have

$$\varphi(\zeta)=\pm\sqrt{-\frac{6k^{2}B\rho_{2}}{A}}F(\zeta),\qquad \zeta=\frac{k\xi^{\alpha}-k^{3}B\rho_{1}\tau^{\alpha}}{\alpha}. \tag{54}$$

In general, the solution is represented by Eq (54), which is dependent on the parameters ρ_0, ρ_1, and ρ_2, as well as the function F that corresponds to them. For further information on the F-expansion approach, we suggest consulting reference [47]. Through the use of this method, we are able to get the general exact solution, which encompasses solutions for single and combination Jacobi elliptic functions, solutions for soliton-like functions, solutions for solitary waves, and solutions for trigonometric functions.

Case 1. When $\rho_0=1,\ \rho_1=-(1+m^{2}),\ \rho_2=m^{2},$ and $F(\zeta)=\mathrm{sn}(\zeta,m)$, we have

$$\varphi(\zeta)=\pm\sqrt{-\frac{6k^{2}Bm^{2}}{A}}\mathrm{sn}(\zeta,m),\qquad \zeta=\frac{k\xi^{\alpha}+k^{3}B(1+m^{2})\tau^{\alpha}}{\alpha}. \tag{55}$$

Case 2. When $\rho_0=1-m^{2},\ \rho_1=2m^{2}-1,\ \rho_2=-m^{2},$ and $F(\zeta)=\mathrm{cn}(\zeta,m)$, we have

$$\varphi(\zeta)=\pm\sqrt{\frac{6k^{2}Bm^{2}}{A}}\mathrm{sn}(\zeta,m),\qquad \zeta=\frac{k\xi^{\alpha}+k^{3}B(2m^{2}-1)\tau^{\alpha}}{\alpha}. \tag{56}$$

Case 3. When $\rho_0=m^{2}-1,\ \rho_1=2-m^{2},\ \rho_2=-1,$ and $F(\zeta)=\mathrm{dn}(\zeta,m)$, we have

$$\varphi(\zeta)=\pm\sqrt{\frac{6k^{2}B}{A}}\ \mathrm{dn}(\zeta,m),\qquad \zeta=\frac{k\xi^{\alpha}+k^{3}B(2-m^{2})\tau^{\alpha}}{\alpha}. \tag{57}$$

Case 4. When $\rho_0=1,\ \rho_1=-2,\ \rho_2=1,$ and $F(\zeta)=\tanh(\zeta)$, we have

$$\varphi(\zeta)=\pm\sqrt{-\frac{6k^{2}B}{A}}\ \tanh(\zeta),\qquad \zeta=\frac{k\xi^{\alpha}+2k^{3}B\tau^{\alpha}}{\alpha}. \tag{58}$$

Case 5. When $\rho_0=0,\ \rho_1=1,\ \rho_2=-1,$ and $F(\zeta)=\mathrm{sech}(\zeta)$, we have

$$\varphi(\zeta)=\pm\sqrt{\frac{6k^{2}B}{A}}\ \mathrm{sech}(\zeta),\qquad \zeta=\frac{k\xi^{\alpha}-k^{3}B\tau^{\alpha}}{\alpha}. \tag{59}$$

And so on. The outcomes obtained for α=1 match the solutions found using the mKdV equation, which match the solutions that were found earlier. The way the fractional mKdV equation was made makes sense now that this has been found. It also proves that these ways work better and are more effective. These results support the framework even more by showing how it is based on sound theory and how important fractional calculus is for adding to and strengthening traditional results

when fractional ordering is needed. The data that were obtained also support the framework. Being able to study and change wave dynamics is very important for the advancement of scientific knowledge and its use in many fields, such as fluid dynamics, nonlinear optics, and plasma physics, to name a few. This ability is very important in many areas, since it makes it possible to understand science and put it to use in real life.

5.5. Multiple soliton and singular solutions for the space–time fractional mKdV equation

The Hirota bilinear method is utilized to find both solitary soliton and multiple soliton solutions based on the information in [27] and related references. By adding the right ansatz to the bilinear version of Eq (18), it is able to make the process of finding soliton solutions in the nonlinear framework easier. This method allows for a systematic study of solitons' stability and interactions, which helps us understand the underlying dynamics that the equation controls. Moreover, using this technique ensures the accurate implementation of this investigation. It is possible that by examining the expressions that are produced, we may get further knowledge on the mechanisms that govern the synthesis and stability of soliton components. Specifically, this is due to the fact that examining the created expressions enables us to discover essential components that alter the functioning of solitons' components. These discoveries have major implications for domains such as fluid dynamics and optical communications, where soliton structures have a considerable impact on the movement of waves and the transmission of information. These fields include fluid dynamics and optical communications. When it comes to these features, the way in which information is moved from one region to another is of particular relevance. Moreover, we must keep in mind that this kind of query might have enormous implications. The investigation of a variety of solutions provides significant insights into the physical consequences of those solutions and reveals prospective applications in the fields of engineering and technology. The use of this strategy not only results in the production of novel ideas that may be utilized in practical settings, but it also contributes to the enhancement of our theoretical comprehension of nonlinear solitons' activity. For instance, systems that make use of solitons in order to expedite the transmission of information are one illustration of this phenomenon. Further inquiry may reveal other connections between solitons' occurrences and other complex systems. It is not feasible to entirely exclude the likelihood that this is the situation. By augmenting both theoretical and practical investigations, this will eventually provide research of superior quality than previously achievable. Hirota's bilinear technique provides a stringent framework for examining the fundamental structure and dynamics of soliton solutions to the space–time fractional mKdV equation.

5.5.1. The fractional Hirota bilinear formalism

This methodology is known as the Hirota bilinear formalism or the Hirota direct technique. A fundamental prerequisite for using this approach is the capacity to convert the FDE into a bilinear form. Hirota demonstrated that soliton solutions may be expressed as polynomials of exponentials inside this bilinear framework. Nonetheless, identifying bilinear formulations of nonlinear FDEs (when they are present) can be very challenging. The Hirota bilinear method is primarily helpful for addressing multiple soliton solutions in diverse nonlinear evolution equations [23,27,28,32,36]. The conventional elucidation of the fractional Hirota bilinear equations is

$$D_x^{\overbrace{\alpha\ldots\alpha}^{n\ times}} D_t^{\overbrace{\alpha\ldots\alpha}^{m\ times}} (P\cdot Q) = \left(D_x^{\alpha} - D_{x'}^{\alpha}\right)^n \left(D_t^{\alpha} - D_{t'}^{\alpha}\right)^m P(t^{\alpha}, x^{\alpha}) Q(t'^{\alpha}, x'^{\alpha})\big|_{x=x',t=t'}.$$

Below, we present some of the bilinear fractional differential operators:

$$\begin{aligned}
&D_x^{\alpha}(P\cdot Q) = (D_x^{\alpha}P)Q - PD_x^{\alpha}Q,\\
&D_x^{\alpha\alpha}(P\cdot Q) = (D_x^{\alpha\alpha}P)Q - 2D_x^{\alpha}PD_x^{\alpha}Q + PD_x^{\alpha\alpha}Q,\\
&D_x^{\overbrace{\alpha\alpha\ \ldots\alpha}^{n\ times}}(Q\cdot Q) = 0, \text{ for } n \text{ is odd},\\
&D_x^{\alpha}D_t^{\alpha}(P\cdot Q) = D_x^{\alpha}((D_t^{\alpha}P)Q - PD_t^{\alpha}Q)\\
&\qquad\qquad = (D_x^{\alpha}D_t^{\alpha}P)Q - D_t^{\alpha}PD_x^{\alpha}Q - D_x^{\alpha}PD_t^{\alpha}Q + PD_x^{\alpha}D_t^{\alpha}Q,\\
&D_x^{\alpha}D_t^{\alpha}(Q\cdot Q) = 2(QD_x^{\alpha}D_t^{\alpha}Q - D_x^{\alpha}Q\,D_t^{\alpha}Q,\\
&D_x^{\overbrace{\alpha\ldots\alpha}^{4\ times}}(P\cdot Q) = (D_x^{\overbrace{\alpha\ldots\alpha}^{4\ times}}P)Q - 4D_x^{\alpha\alpha\alpha}PD_x^{\alpha}Q + 6D_x^{\alpha\alpha}PD_x^{\alpha\alpha}Q - 4D_x^{\alpha}PD_x^{\alpha\alpha\alpha}Q + PD_x^{\overbrace{\alpha\ldots\alpha}^{4\ times}}Q,
\end{aligned}$$

Moreover, the properties of the fractional operators are as follows:

$$\begin{aligned}
&\frac{D_t^{\alpha\alpha}f\cdot f}{f^2} = \iint D_t^{\alpha\alpha}\varphi dx^{\alpha}dx^{\alpha}, \qquad \frac{D_x^{\alpha\alpha}f\cdot f}{f^2} = \varphi,\\
&\frac{D_t^{\alpha}D_x^{\alpha\alpha\alpha}f\cdot f}{f^2} = D_t^{\alpha}D_x^{\alpha}\varphi + 3\varphi\int x\ D_t^{\alpha}\varphi\, dx'^{\alpha},\\
&\frac{D_x^{\overbrace{\alpha\ldots\alpha}^{4\ times}}f\cdot f}{f^2} = D_x^{\alpha\alpha}\varphi + 3\varphi^2, \qquad \frac{D_t^{\alpha}D_x^{\alpha}f\cdot f}{f^2} = D_t^{\alpha}D_x^{\alpha}(\ln f^2),\\
&\frac{D_x^{\overbrace{\alpha\ldots\alpha}^{6\ times}}f\cdot f}{f^2} = D_x^{\overbrace{\alpha..\alpha}^{4\ times}}\varphi + 15\varphi D_x^{\alpha\alpha}\varphi + 15\varphi^3,
\end{aligned}$$

with $\varphi(t^{\alpha}, x^{\alpha}) = 2D_x^{\alpha\alpha}(\ln f(t^{\alpha}, x^{\alpha}))$. For example, the fractional space–time KdV model

$$D_t^{\alpha}\varphi + 6\varphi D_x^{\alpha}\varphi + D_x^{\alpha\alpha\alpha}\varphi = 0,$$

can be converted into the fractional bilinear form as follows:

$$(D_x^{\alpha}D_t^{\alpha} + D_x^{\overbrace{\alpha\ldots\alpha}^{4\ times}})f\cdot f = 0, \qquad \varphi = 2D_x^{\alpha\alpha}(\ln f).$$

5.5.2. Solutions of the space–time fractional mKdV equation

The bilinear approach of the space–time fractional mKdV (Eq (18)) can be written directly in the stretched variables (ξ,τ) as follows:

$$(D_{\tau}^{\alpha} + B\,D_{\xi}^{\alpha\alpha\alpha})g\cdot f = 0, \qquad D_{\xi}^{\alpha\alpha}(f\cdot f + g.g) = 0, \qquad \varphi(\tau,\xi) = R\left(\tan^{-1}\left(\frac{f(\tau,\xi)}{g(\tau,\xi)}\right)\right)_{\xi}.$$

Henceforth, we will replace

$$\varphi(\tau,\xi)=e^{(k_i\xi^{\alpha}-\omega_i\tau^{\alpha})/\alpha}, \tag{60}$$

in the linear expressions of Eq (18) to compute the relative dispersion between the parameters k_i and ω_i. This substitution allows us to derive the dispersion relation, which is given by

$$\omega_i=k_i^3B. \tag{61}$$

This relation characterizes the propagation of solitons in the fractional mKdV equation, linking the wave number k to the frequency ω. The dispersion relation plays a crucial role in understanding the interaction and stability of solitons in the model. As a result, we have the following phase variables for the soliton solution:

$$\theta_i=(k_i\xi^{\alpha}-k_i^3B\,\tau^{\alpha})/\alpha\,. \tag{62}$$

The multiple soliton solutions of the space–time fractional mKdV model (18) are assumed by Hirota's technique to be the formula

$$\varphi(\tau,\xi)=R\left(\tan^{-1}\left(\frac{f(\tau,\xi)}{g(\tau,\xi)}\right)\right)_{\xi}=R\,\frac{gf_{\xi}-f\,g_{\xi}}{f^2+g^2}. \tag{63}$$

Thus, the functions $f(\tau,\xi)$ and $g(\tau,\xi)$ of one soliton solution take the formulae

$$f(\tau,\xi)=e^{\theta_1}=e^{(k_1\xi^{\alpha}-k_1^3B\tau^{\alpha})/\alpha},\qquad g(\tau,\xi)=1. \tag{64}$$

Substituting (63) and (64) into (18) and solving for R, we get

$$R=2\sqrt{\frac{6B}{A}}\,. \tag{65}$$

Combining Eqs (63)–(65) yields one soliton solution

$$\varphi(\tau,\xi)=2\sqrt{\frac{6B}{A}}\,\frac{k_1e^{(k_1\xi^{\alpha}-k_1^3B\,\tau^{\alpha})/\alpha}}{1+e^{2(k_1\xi^{\alpha}-k_1^3B\,\tau^{\alpha})/\alpha}}\,. \tag{66}$$

For the two-soliton solution, we set the auxiliary function

$$f=e^{\theta_1}+e^{\theta_2},\qquad g=1-a_{12}e^{\theta_1+\theta_2},\qquad \theta_i=(k_i\xi^{\alpha}-k_i^3B\,\tau^{\alpha})/\alpha,\quad i=1,2. \tag{67}$$

Using (67) in (63) and putting the results in (18), we have the phase shift coefficient

$$a_{12} = \frac{\left(k_1 - k_2\right)^2}{\left(k_1 + k_2\right)^2}. \tag{68}$$

Henceforth we write the phase shifts as

$$a_{ij} = \frac{\left(k_i - k_j\right)^2}{\left(k_1 + k_j\right)^2}, \qquad 1 \le i < j \le 3. \tag{69}$$

We point out that the space–time fractional mKdV Eq (18) does not show any resonant phenomenon because the phase shift term a_{12} in (68) cannot be 0 or ∞ for $|k_1| \neq |k_2|$. Joining (67) and (68) and substituting the outcome into (63), we have the two-soliton solution.
For the three-soliton solution, we put

$$f = e^{\theta_1} + e^{\theta_2} + e^{\theta_3} - b_{123}e^{\theta_1+\theta_2+\theta_3},\ g = 1 - a_{12}e^{\theta_1+\theta_2} - a_{23}e^{\theta_2+\theta_3} - a_{13}e^{\theta_1+\theta_3},\ \theta_i = (k_i\xi^\alpha - k_i^3 B\,\tau^\alpha)/\alpha,\ i = 1,2,3. \tag{70}$$

Following the same method as previously stated, we obtain

$$b_{123} = a_{12}a_{23}a_{13}. \tag{71}$$

We follow the same steps as described above, except the function

$$\varphi(\tau,\xi) = R\left(\ln\left(\frac{f(\tau,\xi)}{g(\tau,\xi)}\right)\right)_\xi = R\,\frac{g f_\xi - f\ g_\xi}{f\ g}, \tag{72}$$

$f(\tau,\xi)$ and $g(\tau,\xi)$ for the one-singular soliton solution is written as

$$f(\tau,\xi) = 1 + e^{\theta_1} = 1 + e^{(k_1\xi^\alpha - k_1^3 B\,\tau^\alpha)/\alpha}, \qquad g(\tau,\xi) = 1 - e^{\theta_1} = 1 - e^{(k_1\xi^\alpha - k_1^3 B\,\tau^\alpha)/\alpha}. \tag{73}$$

We can construct the singular one soliton solution as follows:

$$\varphi(\tau,\xi) = 2\sqrt{\frac{6B}{A}}\,\frac{k_1 e^{(k_1\xi^\alpha - k_1^3 B\,\tau^\alpha)/\alpha}}{1 - e^{2(k_1\xi^\alpha - k_1^3 B\,\tau^\alpha)/\alpha}}. \tag{74}$$

To construct the singular two-soliton solution, we put

$$f = 1 + e^{\theta_1} + e^{\theta_2} + a_{12}e^{\theta_1+\theta_2},\quad g = 1 - e^{\theta_1} - e^{\theta_2} + a_{12}e^{\theta_1+\theta_2},\ \theta_i = (k_i\xi^\alpha - k_i^3 B\,\tau^\alpha)/\alpha,\ \ i = 1,2. \tag{75}$$

To obtain a singular three-soliton solution, we use

$$
\begin{aligned}
f &= 1+e^{\theta_1}+e^{\theta_2}+e^{\theta_3}+a_{12}e^{\theta_1+\theta_2}+a_{23}e^{\theta_2+\theta_3}+a_{13}e^{\theta_1+\theta_3}+b_{123}e^{\theta_1+\theta_2+\theta_3},\\
g &= 1-e^{\theta_1}-e^{\theta_2}-e^{\theta_3}+a_{12}e^{\theta_1+\theta_2}+a_{23}e^{\theta_2+\theta_3}+a_{13}e^{\theta_1+\theta_3}-b_{123}e^{\theta_1+\theta_2+\theta_3},\\
\theta_i &= (k_i\xi^{\alpha}-k_i^3B\,\tau^{\alpha})/\alpha,\ \ b_{123}=a_{12}a_{23}a_{13},\ i=1,2,3.
\end{aligned}
\tag{76}
$$

Correspondingly, we have

$$
a_{ij}=\frac{\left(k_i-k_j\right)^2}{\left(k_1+k_j\right)^2},\qquad 1\le i<j\le 3. \tag{77}
$$

To validate the special cases of the present model, we first examine the limit α→1, for which the conformable fractional mKdV equation reduces exactly to the classical mKdV equation. In this limit, the solitary, periodic, and kink-type solutions derived in Sections 4 and 5 coincide with the well-known solutions obtained through the inverse scattering, Hirota bilinearization, and Jacobi elliptic function methods. This provides a direct analytical check of consistency. Additionally, the dispersion relation, amplitude–velocity scaling, and wave width dependence recover the classical mKdV equation reported in Ref. [23]. The purpose of developing the new space–time fractional mKdV model is to incorporate anomalous scaling effects that arise in non-Maxwellian, weakly collisional, or turbulent plasma environments while still retaining an analytically tractable evolution equation. The fractional embedding produces a continuous family of nonlinear–dispersive balances parameterized by α, which cannot be captured by classical integer-order models. This enriches the catalog of exact solutions (particularly the soliton, kink, and periodic families) and provides explicit analytical formulas for amplitude–width modulation, phase shifts, and wave steepening behavior that were not available in earlier studies. These results can be used to benchmark numerical solvers, interpret satellite and laboratory observations where departures from classical mKdV behavior have been reported, and guide future extensions to more realistic fractional operators, multi-dimensional geometries, and stability analyses.

In conclusion, the present work complements and extends the existing literature by providing (i) analytically validated reductions in special cases, (ii) explicit comparisons with the classical and fractional mKdV models, (iii) new fractional traveling wave and multi-soliton solutions, and (iv) physically motivated insights into how fractional effects modulate nonlinear ion-acoustic structures. The framework offers a foundation for future theoretical, numerical, and experimental studies aimed at understanding nonlinear wave propagation in complex plasma environments.

5.6. Physical interpretation

The fractional mKdV framework clarifies how nonlinearity and dispersion conspire to shape ion-acoustic structures in magnetized, multi-component plasmas.

(i) Roles of A and B. The coefficient A scales the cubic nonlinearity $\varphi^2\varphi_\xi$; a larger A suppresses the soliton's amplitude for a fixed spectral parameter, while B sets the dispersive length–time scales. Thus, increasing B broadens and accelerates coherent structures, whereas increasing A favors gentler, lower-amplitude profiles.

(ii) Bright vs. kink families. The sign pairing of nonlinearity and dispersion determines the waveform branch: Focusing signatures (effective $A/B > 0$) support bright/dark sech pulses and cnoidal/dnoidal

wavetrains; defocusing signatures (effective $A/B < 0$) generate kink/antikink fronts (tanh) and sn-type periodic waves. In phase space, these correspond to homoclinic (bright) versus heteroclinic (kink) orbits of the traveling wave ODE, with periodic orbits filling the surrounding energy levels.

(iii) Effect of the fractional order α. Decreasing α systematically reduces the peak amplitude and increases the width, reflecting an effective enhancement of dispersive transport relative to nonlinearity. Geometrically, separatrices inflate and fixed-energy loops flatten, yielding lower, broader solitary waves and softer kink fronts. As $\alpha \to 1$, all families converge to their classical mKdV limits, providing a consistency check.

(iv) Interaction physics. In the focusing regime, two-soliton collisions remain elastic: Individual amplitudes and velocities are preserved, while the positions experience logarithmic phase shifts determined solely by the spectral parameters; this persists under fractional dynamics, though reduced a α weakly lengthens interaction ranges via broader tails.

(v) Mapping to observables. The amplitudes set the electrostatic potential or density perturbation levels, the widths map to Debye-scaled interface thickness, and the speeds furnish drift rates that are measurable by in situ probes. The predicted α-dependence implies that environments with stronger locality (e.g., non-Maxwellian tails, collisionality with long waiting times) should exhibit lower, wider solitary structures under comparable background conditions.

(vi) Design and control. The closed-form amplitude–width–speed scalings provide "knobs" for tailoring nonlinear wave packets. Adjusting B (effective dispersion) or operationally mimicking a lower α can be used to mitigate steep gradients, whereas increasing A (relative nonlinearity) sharpens the interfaces.

(vii) Limitations and scope. Strongly local kernels or multi-scale kinetic effects may require alternative fractional definitions or kinetic closures. Within its validity range, the present interpretation links the parameters (A,B,α) to observable morphology and interaction outcomes, offering a transparent bridge from mathematical solutions to experimental diagnostics and numerical benchmarking.

Ion-acoustic solitary structures in magnetized, multi-component plasmas frequently display behaviors that deviate from the predictions of classical (integer-order) KdV/mKdV models (such as anomalous dispersion, broadened electrostatic pulses, and amplitude attenuation). These features commonly arise in environments where weak collisionality, turbulence, superthermal particle populations, and nonlocal transport effects are present. Classical models cannot fully capture these effects because they rely on strict locality and integer-order derivatives. Fractional modeling provides a natural extension, but most existing approaches use Caputo or Riemann–Liouville derivatives, which introduce nonlocal integral kernels that (i) complicate the dispersion relations, (ii) disrupt reductive perturbation expansions, and (iii) rarely yield closed-form soliton or periodic solutions.

The motivation of this work is to bridge this methodological and physical gap by developing a dispersion-consistent and physically transparent space–time fractional mKdV model using the conformable derivative. Unlike integral-based fractional operators, the CFD preserves the chain rule and product rule, allowing a rigorous reductive perturbation derivation, direct traveling wave reduction, and the construction of exact analytical solutions (soliton, kink, and Jacobi elliptic waves). This enables us to quantify how the fractional order α modulates the waves' amplitude, width, steepness, and interaction properties (effects that cannot be captured by classical integer-order equations).

The relevance of the present results to laboratory and space plasmas is supported by a quantitative comparison with observed parameter regimes. Laboratory experiments (Q-machines, double-plasma devices) typically operate at densities of 10^8–10^{10} cm^{-3}, electron temperatures of 0.1–1 eV, and magnetic fields of B∼0.01–0.1 T, with Mach numbers of 1.1–2.0. These values correspond directly to the sign and magnitude of the nonlinear and dispersive coefficients A and B in our fractional mKdV

model. Likewise, spacecraft observations (Cluster, THEMIS) routinely detect solitary and steepened ion-acoustic structures with amplitudes of 0.1–1 V and characteristic lengths near the Debye scale. The variability and departures from classical behavior in these regions (driven by turbulence, superthermal electrons, and weak collisions) are consistent with the fractional-order correction encoded through α, which represents controlled deviations from classical local transport.

The analytical soliton, kink, and periodic solutions derived from the space–time fractional mKdV equation possess direct relevance to real plasma environments. In laboratory devices such as Q-machines and double-plasma experiments, ion-acoustic solitary structures are routinely observed, with measured amplitudes, widths, and propagation speeds that correspond one-to-one with the parameters of the analytical waveforms presented here. Likewise, spacecraft missions (including Cluster, THEMIS, and MMS) regularly detect electrostatic solitary waves, steepened fronts, and periodic wave trains whose morphology reflects the same balance of nonlinearity and dispersion encoded in the mKdV framework. The fractional order α provides a controlled means of capturing deviations from classical behavior caused by turbulence, weak collisionality, or superthermal electron populations, enabling a physically interpretable mapping between observed waveform broadening or amplitude attenuation and the underlying plasma conditions. Thus, the solutions obtained in this work not only furnish exact analytical benchmarks for numerical solvers but also serve as practical diagnostic tools for interpreting laboratory measurements and in situ satellite observations of nonlinear ion-acoustic wave phenomena.

Thus, the contribution of this paper is twofold: (1) To provide a rigorous, analytically solvable fractional mKdV framework that captures physically observed deviations from classical behavior, and (2) to deliver exact solutions and scaling laws that can serve as benchmarks for interpreting laboratory experiments, comparisons with spacecraft measurements, and validating numerical fractional PDE solvers.

6. Conclusions

This paper developed a dispersion-consistent, space–time fractional mKdV framework (with laboratory variables) to model ion-acoustic structures in magnetized, multi-component plasmas with local fractional effects. Using conformable fractional operators, we derived a reduced evolution equation in which the roles of nonlinearity A and dispersion B remain explicit. This transparency enabled closed-form amplitude–width–speed scalings and a clear separation of the physical effects: A sets the nonlinear intensity scale, while B fixes the spatiotemporal dispersion. Within this setting, we constructed complementary families of exact traveling waves (bright/dark sech solitons, kink/antikink fronts, and Jacobi elliptic (sn/cn/dn) wavetrains) via direct integration, elliptic reductions, and Hirota's bilinear formalism (including explicit one- and two-soliton solutions and phase shifts written directly in $(x,t;A,B)$ form). A phase portrait and bifurcation analysis of the traveling wave ODE linked these solutions to homoclinic, heteroclinic, and periodic orbits, providing a geometric classification that clarifies parameter regimes and limiting connections. Across all branches, the fractional order α plays a systematic, measurable role: Decreasing α lowers the peak amplitude and broadens the profile (reflecting an effective strengthening of dispersive transport relative to nonlinearity), while the classical solutions are recovered smoothly as $\alpha = 1$, furnishing an internal consistency check.

Beyond exact solutions, the paper contributes practical tools and benchmarks. First, the explicit two-soliton formulas in physical units facilitate a direct comparison between simulations and experiments without back-transformation from normalized variables. Second, the phase portrait templates and energy-level interpretations offer diagnostics for identifying wave families and

transition mechanisms in data. Third, the analytic scalings provide "design knobs" for tailoring solitary interfaces, which would be useful for numerical verification, laboratory planning, and the interpretation of space plasma observations.

Several limitations delimit the present study. The conformable derivative captures fractional calculus in a tractable, local-in-form sense; strongly nonlocal kernels (e.g., Caputo/Riemann–Liouville with history integrals) or kinetic closures may be required to describe heavy-tailed waiting times and velocity–space anisotropies more faithfully. The analysis focused on one-dimensional, weakly nonlinear regimes; transverse effects, multi-dimensional instabilities, and turbulence–coherent structure interactions remain open. Dissipation, external noise, and strong inhomogeneity were not treated in detail, and could modify the collisions' elasticity and long-time coherence.

These caveats point to fertile directions for future work: (i) Extending the conformable framework to alternative fractional definitions and comparing its predictive ability against experiments and kinetic simulations; (ii) generalizing to higher-dimensional ZK-type (mZK-type) models and exploring modulational instability and envelope dynamics in fractional media; (iii) incorporating weak dissipation/forcing and stochasticity to chart transition routes beyond integrability; (iv) coupling to data-driven closures (e.g., neural operators) for parameter inference and uncertainty quantification; and (v) designing targeted experiments (or mission data analyses) to test the predicted α-dependent amplitude–width trends and soliton phase shifts. In summary, this study provides an application-ready analytical foundation that unifies fractional calculus, exact nonlinear wave theory, and physically interpretable parametrizations, and it opens a path to quantitatively connect fractional-order effects with observable solitary structures in the laboratory and space plasmas.

Future work

Building on the results of this manuscript, several directions merit investigation:

(1) Alternative fractional operators: Benchmark conformable derivatives against the Caputo, Riemann–Liouville, Atangana–Baleanu, and tempered models to quantify how the fractional order alters amplitude–width-speed scalings, the collisions' elasticity, and dispersion.

(2) To demonstrate the well-posedness, regularity, and conserved values for the fractional mKdV equation, it is necessary to conduct a comprehensive analysis. Additionally, it is necessary to develop spectral and Evans-function approaches in order to evaluate the stability of solitary waves across the whole range of α.

(3) Multidimensional extensions: Derive and study fractional ZK/KP-type equations, examining transverse stability, filamentation, and oblique propagation in magnetized plasmas.

(4) Modulation theory: Formulate fractional Whitham equations to predict the slow evolution of cnoidal/kink lattices and to chart modulational instability thresholds versus α.

(5) Nonintegrable perturbations: Include weak dissipation, inhomogeneity, and stochastic forcing; analyze solitons' radiation, capture/repulsion, and long-time coherence using Melnikov and multi-scale methods.

(6) Data-constrained modeling: Couple the analytic solutions with inversion to infer (A,B,α) from laboratory or spacecraft time series; leverage neural operators to emulate the fractional dynamics for fast forecasting.

(7) High-order numerics: Design energy-stable, structure-preserving schemes and validate them against the closed-form one- and two-soliton benchmarks provided here.

(8) Kinetic closures: Connect fractional transport to the underlying Vlasov–Fokker–Planck kinetics (e.g., continuous-time random walks, kappa tails), deriving α and the coefficients from microscopic parameters.
(9) Experiment/mission links: Propose diagnostics to test the predicted α-dependent amplitude broadening and phase shifts, and curate comparison datasets from auroral and laboratory measurements.
(10) Interaction networks: Study multi-soliton gases and turbulence–coherent structure coupling in the fractional regime, seeking reduced statistical descriptions (generalized kinetic equations) that are sensitive to fractional-order effects.

Use of Generative-AI tools declaration

The author hereby declares that artificial intelligence tools were used in this research only as supportive instruments for tasks such as language refinement, idea organization, and data summarization. All intellectual contributions, critical analysis, and final interpretations are solely our own. The use of AI has been properly documented to maintain transparency and uphold academic integrity.

Acknowledgments

The researcher would like to thank the Deanship of Graduate Studies and Scientific Research at Qassim University for financial support (QU-APC-2025).

Conflict of interest

The author declares that they have no conflicts of interest.

References

1. H. Washimi, T. Taniuti, Propagation of ion-acoustic solitary waves of small amplitude, *Phys. Rev. Lett.*, **17** (1966), 996–998. https://doi.org/10.1103/PhysRevLett.17.996
2. A. Mushtaq, H. A. Shah, Nonlinear Zakharov–Kuznetsov equation for obliquely propagating two-dimensional ion-acoustic waves in a relativistic, rotating magnetized electron–positron–ion plasma, *Phys. Plasmas*, **12** (2005), 072306. https://doi.org/10.1063/1.1946729
3. T. S. Gill, A. Singh, H. Kaur, N. S. Saini, P. Bala, Ion-acoustic solitons in weakly relativistic plasma containing electron–positron and ion, *Phys. Lett. A*, **361** (2007), 364–367. https://doi.org/10.1016/j.physleta.2006.09.053
4. R. S. Tiwari, Ion-acoustic dressed solitons in electron–positron–ion plasmas, *Phys. Lett. A*, **372** (2008), 3461–3466. https://doi.org/10.1016/j.physleta.2008.02.002
5. H. Pakzad, Ion acoustic solitary waves in plasma with nonthermal electron and positron, *Phys. Lett. A*, **373** (2009), 847–850. https://doi.org/10.1016/j.physleta.2008.12.066
6. S. Mahmood, A. Mushtaq, H. Saleem, Ion acoustic solitary wave in homogeneous magnetized electron–positron–ion plasmas, *New J. Phys.*, **5** (2003), 1–28. https://doi.org/10.1088/1367-2630/5/1/328
7. R. Tiwari, A. Kaushik, M. Mishra, Effects of positron density and temperature on ion acoustic dressed solitons in an electron–positron–ion plasma, *Phys. Lett. A*, **365** (2007), 335–340. https://doi.org/10.1016/j.physleta.2007.01.020

8. M. A. Moghanjoughi, Effects of ion-temperature on propagation of the large-amplitude ion-acoustic solitons in degenerate electron–positron–ion plasmas, *Phys. Plasmas*, **17** (2010), 082315. https://doi.org/10.1063/1.3480117
9. A. Shah, R. Saeed, M. Noaman-ul-Haq, Nonplanar converging and diverging shock waves in the presence of thermal ions in electron–positron plasma, *Phys. Plasmas*, **17** (2010), 072307. https://doi.org/10.1063/1.3457928
10. A. E. Kalejahi, M. Mehdipoor, M. A. Moghanjoughi, Effects of positron density and temperature on ion-acoustic solitary waves in a magnetized electron–positron–ion plasma: Oblique propagation, *Phys. Plasmas*, **16** (2009), 052309. https://doi.org/10.1063/1.3142465
11. S. A. Colgate, H. Li, V. Pariev, The origin of the magnetic fields of the universe: The plasma astrophysics of the free energy of the universe, *Phys. Plasmas*, **8** (2001), 2425–2431. https://doi.org/10.1063/1.1351827
12. M. M. Rahman, A. A. Mamun, M. S. Alam, Positron acoustic shock waves in four-component plasmas with nonthermal electrons and positrons, *J. Korean Phys. Soc.*, **64** (2014), 1828–1833. https://doi.org/10.3938/jkps.64.1828
13. B. B. Mouhammadoul, A. Alim, C. G. L. Tiofack, A. Mohamadou, Modulated positron-acoustic waves and rogue waves in a magnetized plasma system with nonthermal electrons and positrons, *Astrophys. Space Sci.*, **365** (2020), 90. https://doi.org/10.1007/s10509-020-03805-6
14. W. Alhejaili, D. V. Douanla, A. Alim, C. G. L. Tiofack, A. Mohamadou, S. A. E. Tantawy, Multidimensional dust-acoustic rogue waves in electron-depleted complex magnetoplasmas, *Phys. Fluids*, **35** (2023), 063102. https://doi.org/10.1063/5.0153338
15. C. G. L. Tiofack, D. V. Douanla, A. Alim, A. Mohamadou, S. M. E. Ismaeel, S. A. E. Tantawy, Dust-acoustic modulated structures in self-gravitating magnetized electron-depleted dusty plasmas: Multi-rogue waves and dark soliton collisions, *Eur. Phys. J. Plus*, **136** (2021), 699. https://doi.org/10.1140/epjp/s13360-021-01686-4
16. D. V. Douanla, C. G. L. Tiofack, A. Alim, A. Mohamadou, H. A. Alyousef, S. M. E. Ismaeel, et al., Dynamics and head-on collisions of multidimensional dust acoustic shock waves in a self-gravitating magnetized electron-depleted dusty plasma, *Phys. Fluids*, **35** (2023), 023103. https://doi.org/10.1063/5.0137914
17. Shalini, N. S. Saini, Ion acoustic solitary waves and double layers in a plasma with two temperature electrons featuring Tsallis distribution, *Phys. Plasmas*, **21** (2014), 102901. https://doi.org/10.1063/1.4897177
18. Shalini, N. S. Shalini, A. P. Misra, Modulation of ion-acoustic waves in a nonextensive plasma with two-temperature electrons, *Phys. Plasmas*, **22** (2015), 092124. https://doi.org/10.1063/1.4931074
19. G. S. Lakhina, A. P. Kakad, S. V. Singh, F. Verheest, Ion- and electron-acoustic solitons in two-electron temperature space plasmas, *Phys. Plasmas*, **15** (2008), 062903. https://doi.org/10.1063/1.2930469
20. A. Saha, J. Tamang, Qualitative analysis of the positron-acoustic waves in electron-positron-ion plasmas with deformed Kaniadakis distributed electrons and hot positrons, *Phys. Plasmas*, **24** (2017), 082101. https://doi.org/10.1063/1.4994396
21. M. Ferdousi, S. Yasmin, S. Ashraf, A. A. Mamun, Nonlinear propagation of ion-acoustic waves in an electron-positron-ion plasma, *Astrophys. Space Sci.*, **352** (2014), 579–584. https://doi.org/10.1007/s10509-014-1950-7
22. S. A. E. Tantawy, Nonlinear dynamics of soliton collisions in electronegative plasmas: The phase shifts of the planar KdV- and mKdV-soliton collisions, *Chaos Soliton. Fract.*, **93** (2016), 162–168. https://doi.org/10.1016/j.chaos.2016.10.011

23. A. H. Almuqrin, D. V. Douanla, G. L. C. Tiofack, A. Mohamadou, S. M. E. Ismaeel, S. A. El-Tantawy, On the propagation and interaction of the low-frequency ion-acoustic multi-solitons in a magnetoplasma having nonextensive electrons using Hirota bilinear method, *J. Low Freq. Noise V. A.*, **44** (2025), 1612–1630. https://doi.org/10.1177/14613484251337289
24. A. Saha, Bifurcation of travelling wave solutions for the generalized KP–MEW equations, *Commun. Nonlinear Sci.*, **17** (2012), 3539–3551. https://doi.org/10.1016/j.cnsns.2012.01.005
25. Z. Li, Traveling wave solutions, numerical simulation and phase portraits for the conformable space-time fractional diffusive predator–prey system, *Phys. Lett. A*, **561** (2025), 130995. https://doi.org/10.1016/j.physleta.2025.130995
26. S. Akram, J. Ahmad, S. U. Rehman, S. Alkarni, N. A. Shah, Exploration of solitary wave solutions of highly nonlinear KdV–KP equation arising in water waves and stability analysis, *Results Phys.*, **54** (2023), 107054. https://doi.org/10.1016/j.rinp.2023.107054
27. A. M. Wazwaz, The simplified Hirota's method for studying three extended higher-order KdV-type equations, *J. Ocean Eng. Sci.*, **1** (2016), 181–185. https://doi.org/10.1016/j.joes.2016.06.003
28. K. J. Wang, Resonant multiple wave, periodic wave and interaction solutions of the new extended (3+1)-dimensional Boiti–Leon–Manna–Pempinelli equation, *Nonlinear Dynam.*, **111** (2023), 16427–16439. https://doi.org/10.1007/s11071-023-08699-x
29. H. H. Sheng, G. F. Yu, Solitons, breathers and rational solutions for a (2+1)-dimensional dispersive long wave system, *Physica D*, **432** (2022), 133140.
30. S. S. Zhang, T. Xu, M. Li, X. F. Zhang, Higher-order algebraic soliton solutions of the Gerdjikov–Ivanov equation: Asymptotic analysis and emergence of rogue waves, *Physica D*, **432** (2022), 133128. https://doi.org/10.1016/j.physd.2021.133128
31. K. A. Alsatami, Analysis of solitary wave behavior under stochastic noise in the generalized Schamel equation, *Sci. Rep.*, **15** (2025), 19157. https://doi.org/10.1038/s41598-025-04696-9
32. A. A. Hassaballa, M. Yavuz, G. A. M. O. Farah, F. A. Almulhim, S. A. Khalek, E. A. B. A. Salam, Mathematical modeling of influence of multiplicative white noise on dynamical soliton solutions in the KdV equation, *Math. Open*, **4** (2025), 2550013. https://doi.org/10.1142/S2811007225500130
33. M. Zayed, H. M. AbdelSalam, I. Daqqa, S. A. Khalek, E. A. B A. Salam, G. M. Ismail, Stochastic dynamics of solitary waves in the damped mKdV equation: Analytical solutions and numerical simulations, *AIMS Math.*, **10** (2025), 25907–25938. https://doi.org/10.3934/math.20251145
34. K. J. Wang, A fast insight into the optical solitons of the generalized third-order nonlinear Schrödinger equation, *Results Phys.*, **40** (2022), 105872. https://doi.org/10.1016/j.rinp.2022.105872
35. K. J. Wang, G. D. Wang, Variational theory and new abundant solutions to the (1+2)-dimensional chiral nonlinear Schrödinger equation in optics, *Phys. Lett. A*, **412** (2021), 127588. https://doi.org/10.1016/j.physleta.2021.127588
36. K. J. Wang, The generalized (3+1)-dimensional B-type Kadomtsev–Petviashvili equation: Resonant multiple soliton, N-soliton, soliton molecules and interaction solutions, *Nonlinear Dynam.*, **112** (2024), 7309–7324. https://doi.org/10.1007/s11071-024-09356-7
37. T. Aboelenen, Local discontinuous Galerkin method for distributed-order time and space-fractional convection–diffusion and Schrödinger-type equations, *Nonlinear Dynam.*, **92** (2018), 395–413. https://doi.org/10.1007/s11071-018-4063-y
38. Y. Liang, K. Wang, Dynamics of the new exact wave solutions to the local fractional Vakhnenko–Parkes equation, *Fractals*, 2025. https://doi.org/10.1142/S0218348X25501026
39. K. J. Wang, The fractal active low-pass filter within the local fractional derivative on the Cantor set, *COMPEL*, **42** (2023), 1396–1407. https://doi.org/10.1108/COMPEL-09-2022-0326

40. S. R. Aderyani, R. Saadati, J. Vahidi, J. F. G. Aguilar, The exact solutions of conformable time-fractional modified nonlinear Schrödinger equation by first integral method and functional variable method, *Opt. Quant. Electron.*, **54** (2022), 218. https://doi.org/10.1007/s11082-022-03605-y
41. A. A. Hassaballa, M. Yavuz, E. A. B. A. Salam, G. A. M. O. Farah, I. Daqqa, Geometrical representation and Hirota direct approach for multiple soliton solutions of nonlinear M-coupled fractional equations, *Math. Comp. Model. Dyn.*, **31** (2025), 2595101. https://doi.org/10.1080/13873954.2025.2595101
42. J. Ahmad, S. Akram, S. U. Rehman, N. B. Turki, N. A. Shah, Description of soliton and lump solutions to the M-truncated stochastic Biswas–Arshed model in optical communication, *Results Phys.*, **51** (2023), 106719. https://doi.org/10.1016/j.rinp.2023.106719
43. W. He, N. Chen, I. Dassios, N. A. Shah, J. D. Chung, Fractional system of Korteweg–de Vries equations via Elzaki transform, *Mathematics*, **9** (2021), 673. https://doi.org/10.3390/math9060673
44. N. A. Shah, Y. S. Hamed, K. M. Abualnaja, J. D. Chung, R. Shah, A. Khan, A comparative analysis of fractional-order Kaup–Kupershmidt equation within different operators, *Symmetry*, **14** (2022), 986. https://doi.org/10.3390/sym14050986
45. N. A. Shah, H. A. Alyousef, S. A. E. Tantawy, R. Shah, J. D. Chung, Analytical investigation of fractional-order Korteweg–de Vries-type equations under Atangana–Baleanu–Caputo operator: Modeling nonlinear waves in a plasma and fluid, *Symmetry*, **14** (2022), 739. https://doi.org/10.3390/sym14040739
46. E. A. B. A. Salam, G. F. Hassan, Solutions to class of linear and nonlinear fractional differential equations, *Commun. Theor. Phys.*, **65** (2016), 127. https://doi.org/10.1088/0253-6102/65/2/127
47. M. I. Nouh, Y. A. Azzam, E. A. B. A. Salam, Modeling fractional polytropic gas spheres using artificial neural network, *Neural Comput. Appl.*, **33** (2021), 4533–4546. https://doi.org/10.1007/s00521-020-05277-9
48. E. A. B. A. Salam, M. S. Jazmati, H. Ahmad, Geometrical study and solutions for family of Burgers-like equations with fractional order space-time, *Alex. Eng. J.*, **61** (2022), 511–521. https://doi.org/10.1016/j.aej.2021.06.032
49. R. Khalil, M. A. Horani, A. Yousef, M. Sababheh, A new definition of fractional derivative, *J. Comput. Appl. Math.*, **264** (2014), 65–70. https://doi.org/10.1016/j.cam.2014.01.002
50. E. A. B. A. Salam, M. I. Nouh, E. A. Elkholy, Analytical solution to the conformable fractional Lane–Emden type equations arising in astrophysics, *Sci. Afr.*, **8** (2020), e00386. https://doi.org/10.1016/j.sciaf.2020.e00386
51. I. Jaradat, M. Alquran, Construction of solitary two-wave solutions for a new two-mode version of the Zakharov–Kuznetsov equation, *Mathematics*, **8** (2020), 1127. https://doi.org/10.3390/math8071127

AIMS Press